Moist Potential Vorticity Diagnosis of the Tropical Cyclone Boundary Layer: Influence of Roll Vortices

Ipshita Dey[1] and Morgan O'neill[1]

[1]Stanford University

November 23, 2022

Abstract

Physical processes determining the dynamic and thermodynamic structure of a tropical cyclone boundary layer (TCBL) are quite different from anywhere else in the atmospheric boundary layer due to the substantial contribution of latent heating and frictional convergence. These processes regulate the radial and vertical distributions of momentum and enthalpy fluxes that are closely related to storm development and intensification. Our current understanding of TCBL is limited by the number of observations in this region, and a majority of the observational studies assume an axisymmetric structure. Three-dimensional observations and numerical studies show that substantial asymmetric structure exists in the TCBL. This study investigates the link between the asymmetric structure and small-scale processes using a Moist Potential Vorticity (MPV) framework. The simulated TCBL is uniquely characterized as a region of negative MPV with a robust and coherent layer of high-magnitude negative MPV embedded within, referred to as the Potential Vorticity Minimum Layer (PVML). The PVML can interact with the local flow anomalies such as those associated with roll vortices provided they are vertically collocated. The small-scale dynamical processes set the thermodynamic structure inside the TCBL and this interplay modulates the height of the PVML. Since the height of the PVML combines information about the local wind and thermal structures using a materially conserved variable, it is a valuable proxy to study the evolving 'topography' of a simulated TCBL.

Moist Potential Vorticity Diagnosis of the Tropical Cyclone Boundary Layer: Influence of Roll Vortices

Ipshita Dey and Morgan O'Neill

Department of Earth System Science, Stanford University, Stanford, CA

Corresponding author: Ipshita Dey, ipshidatm@gmail.com

ABSTRACT: Physical processes determining the dynamic and thermodynamic structure of a tropical cyclone boundary layer (TCBL) are quite different from anywhere else in the atmospheric boundary layer due to the substantial contribution of latent heating and frictional convergence. These processes regulate the radial and vertical distributions of momentum and enthalpy fluxes that are closely related to storm development and intensification. Our current understanding of TCBL is limited by the number of observations in this region, and a majority of the observational studies assume axisymmetric structure. Three-dimensional observations and numerical studies show that substantial asymmetric structure exists in the TCBL. This study investigates the link between the asymmetric structure and small-scale processes using a Moist Potential Vorticity (MPV) framework. The simulated TCBL is uniquely characterized as a region of negative MPV with a robust and coherent layer of high-magnitude negative MPV embedded within, referred to as the Potential Vorticity Minimum Layer (PVML). The PVML can interact with the local flow anomalies such as those associated with roll vortices provided they are vertically collocated. The small-scale dynamical processes set the thermodynamic structure inside the TCBL and this interplay modulates the height of the PVML. Since the height of the PVML combines information about the local wind and thermal structures using a materially conserved variable, it is a valuable proxy to study the evolving 'topography' of a simulated TCBL.

1. Introduction

The application of potential vorticity (PV) diagnostics to understand synoptic-scale processes has greatly benefited tropical cyclone (TC) forecasting, particularly in predicting TC motion (Thorpe 1985; Davis and Emanuel 1991; Wu and Emanuel 1993; Shapiro and Franklin 1995; Schubert et al. 1999; Wang and Zhang 2003). Studies have also linked the evolution of upper-level PV anomalies to TC genesis and intensification (Montgomery and Farrell 1993; Molinari et al. 1995). This is possible due to the utility of PV as a materially conserved tracer in the absence of frictional and diabatic forces. Positive diabatic heating on synoptic scales results in the "dilution" of PV substance in the isentropic layers above the heating maximum, and a "concentration" below since there can be no flux of PV across isentropic surfaces, but there can be a flux of mass (Haynes and McIntyre 1987). However, the usefulness of PV in understanding mesoscale processes has been limited, owing largely to the difficulty in characterizing unbalanced motions. At these scales, velocity perturbations are comparable to the balanced velocity field, which introduces strong non-linearities in the equations and makes it impractical to perform PV inversion. Nevertheless, PV still retains its utility in tracking the diabatic and frictional forces (Haynes and McIntyre 1987) as they directly impact the mass and wind field respectively and adjust them locally to a new PV. Recent studies have highlighted the significance of using PV in the study of mesoscale processes (Chagnon and Gray 2009; Shutts 2017; Clarke et al. 2019; Sessions et al. 2019; Harvey et al. 2020). For instance, convective heating in a strongly vertically sheared environment has been shown to create quasi-horizontal PV dipoles that last longer than the convection that initiated them and can initiate new convection (Chagnon and Gray 2009; Weijenborg et al. 2017; Oertel et al. 2019).

Mesoscale processes inside the tropical cyclone boundary layer (TCBL) can regulate the radial and vertical distributions of momentum and enthalpy fluxes that in turn set the necessary boundary conditions for the inversion of a quasi-balanced, zero-PV TC interior, including the eyewall (Emanuel 1986). This has an important implication that the TCBL plays an important role in controlling the TC structure and intensity, as suggested by several studies (Smith et al. 2009; Smith and Montgomery 2015; Persing et al. 2013; Gopalakrishnan et al. 2013) and needs to be accurately represented in numerical models (Emanuel 1995; Braun et al. 2011; Nolan et al. 2009b; Smith and

Thomsen 2010; Kepert 2011; Bryan 2011; Cione et al. 2013; Kilroy et al. 2016; Bu et al. 2017). This includes improved representation of kilometer-scale coherent eddies that are aligned in the mean tangential wind direction known as roll vortices (Wurman and Winslow 1998; Morrison et al. 2005; Lorsolo et al. 2008; Ellis and Businger 2010; Foster 2013). Roll vortices in the TCBL are generally formed as a consequence of inflection point instability (Foster 2005; Nolan 2005; Gao and Ginis 2018) and can assist the intensification process via vertical transport of tangential momentum (Zhang et al. 2008; Gao et al. 2017). Furthermore, the up-gradient transfer of surface heat and momentum fluxes associated with roll vortices can energize the large-scale motions, possibly resulting in increased convective activity (Sukhanovskii and Popova 2020; Sroka and Guimond 2021).

The main purpose of this paper is to characterize the local TCBL dynamics using the relevant PV framework and demonstrate that an accurate analysis of coherent PV structures can provide additional insight into the source, evolution, and maintenance of TCBL processes. The application of traditional dry PV (hereafter referred to as PV) in the TCBL is complicated by moist convection. Latent heating associated with moist convection is itself a source of PV anomalies (Chagnon and Gray 2009). Latent heating/cooling can be incorporated as a source/sink in the thermodynamic equation (θ tendency) but the resulting sources/sinks in PV are small in magnitude and difficult to track (Marquet 2014). In addition, the TCBL is non-uniformly saturated, which points to a horizontal discontinuity in the latent heat term of the thermodynamic equation in the transition regions between saturated air (where latent heat can be released) and unsaturated air (where latent heat cannot be released). Furthermore, there can be latent cooling in unsaturated air due to re-evaporation of falling hydrometeors which may appear as an additional sink term. To address this problem, several formulations of Moist Potential Vorticity (MPV) have been used by replacing potential temperature (θ) with the virtual potential temperature (θ_v), generalized potential temperature (θ^*) or equivalent potential temperature (θ_e) (Bennetts and Hoskins 1979; Emanuel 1979; Schubert et al. 2001; Gao et al. 2004; Marquet 2014).

$$PV_e = \frac{1}{\rho}\zeta_a \cdot \nabla\theta_e \quad (1)$$

$$\theta_e = T\left(\frac{p_d}{p_o}\right)^{\frac{-R_d}{C_{pd}+C_l.q_t}} (H)^{\frac{-q_v R_v}{C_{pd}+C_l.q_t}} exp\left(\frac{L_v q_v}{(C_{pd}+C_l.q_t)T}\right) \quad (2)$$

In this study, we use the formulation (Eq. 1) for MPV that uses the equivalent potential temperature (θ_e). Here, ζ_a is the three-dimensional absolute vorticity and ρ is the total density of moist air. θ_e is defined in Eq. 2 where T is the temperature, p_d is the partial pressure of dry air, p_o is the reference pressure (1000 mb), R_d and R_v are the gas constants for dry air and water vapor respectively, C_{pd} and C_l are the specific heats of dry air at constant pressure and liquid water respectively, q_v is the water vapor mixing ratio, q_t is the total liquid water content per unit mass of dry air and L_v is the latent heat of vaporization. The resultant MPV, hereafter referred to as PV_e and measured in Potential Vorticity Units (PVU), includes the relative humidity (H) to account for both saturated and unsaturated conditions whilst also conserving the total entropy in the absence of external sensible or latent heating (Emanuel 1994). Several other studies have used similar definitions of MPV to investigate frontal rain bands (Bennetts and Hoskins 1979; Emanuel 1979; Cao and Cho 1995; Liang et al. 2010). Schubert et al. (2001) demonstrated that the solenoidal (baroclinic) production of MPV is non-zero for the choice of θ_e (i.e. PV_e is non-invertible) and recommended the use of θ_v instead. However, Wetzel et al. (2020) recently showed that PV_e is, in fact, more suitable to recover the balanced composition of the flow if used with additional balanced moist variables. Since PV inversion in TCBL is neither feasible nor the goal of this study and because the solenoidal production of PV_e can be neglected when compared to frictional and diabatic sources (small magnitudes of pressure and density gradients), PV_e is the more appropriate choice for MPV than PV_v. The choice of PV_e is also supported by the fact that θ_e is linked to the total entropy of the moist system and is conserved for reversible adiabatic motions (no condensate fallout) of saturated air, thereby allowing for meaningful interpretation of diabatic tendencies of PV_e.

2. Model Description

Direct measurements of PV_e in the TCBL are strongly limited due to the lack of observations, particularly high-resolution measurements of winds and thermodynamic properties (Marks et al. 2008; Cione et al. 2020). We instead study the TCBL simulated using an idealized numerical model. Numerical models rely heavily on boundary layer parameterizations developed for moderate wind conditions. The simulated TC intensity is highly sensitive to the choice of the parameterization scheme (Braun and Tao 2000; Nolan et al. 2009a,b; Smith and Thomsen 2010; Kepert 2011; Green and Zhang 2015; Ming and Zhang 2016). This study employs the non-hydrostatic Bryan Cloud Model 1 version 19.8 (Bryan and Rotunno 2009; Bryan and Fritsch 2002) to simulate two idealized TCs on an f-plane, one with a parameterized boundary layer (referred to as "TC-Param") and the other without (referred to as "TC-NonParam"). TC-Param uses the Yonsei University (YSU) scheme (Hong et al. 2006) to parameterize all turbulence whereas TC-NonParam uses the TKE scheme (Deardorff 1980) to treat only the sub-grid turbulent processes. The horizontal resolution needed by mesoscale models to produce realistic TC intensity whilst adequately representing mesoscale features is approximately 5 km (Fierro et al. 2009; Baldauf et al. 2011; Gentry and Lackmann 2010). Both TCs are configured for a doubly periodic domain of 480 km x 480 km with a uniform horizontal grid spacing of 500 m. The vertical domain is split into three layers: (i) bottom layer extending up to 3 km above sea level with a uniform grid spacing of 50 m, (ii) middle layer extending from 3 km to 8.5 km with stretched grid spacing ranging from 50 m to 500 m, and (iii) top layer extending up to 25 km with a uniform grid spacing of 500 m. A vertical sponge layer in the topmost 5 km is used to minimize the reflection and buildup of gravity waves. Both simulations are initiated using a finite-amplitude vortex in an atmosphere that is neutrally stable to moist convection (Rotunno and Emanuel 1987) and an ocean surface with constant sea surface temperature (SST) set to 28$^\circ C$ (or 301 K). A moist tropical sounding (Dunion 2011) is used to prescribe an atmosphere unstable to moist convection and a Newtonian cooling scheme is used to relax the temperature profile towards the initial state over 12 hrs. The initial vortex has an analytic form given by Rotunno and Emanuel (1987) with maximum tangential winds ($U_{t,max}$) of 15 m/s and a radius of maximum winds (RMW) of 82.5 km. The two-moment scheme based on Morrison and Gettelman (2008) has been used to parameterize cloud microphysics and precipitation in both TCs. The Coriolis parameter is set to 0.0002 s^{-1}, which is four times higher than the typical tropical values. This unusually high value was chosen to produce a TC with a relatively smaller wind field as the TC size (D) is bounded by the Coriolis parameter, i.e. $D = \frac{V_p}{f}$ (Emanuel 1986). This allows for a smaller computational domain to encompass the entire TC, thereby reducing the high computational cost (Khairoutdinov and Emanuel 2013).

Large-eddy simulations (LES) of TCBL are becoming an increasingly viable alternative to mesoscale modeling, in which both the radial and vertical turbulent mixing are explicitly simulated without relying on traditional boundary layer approximations (Zhu 2008; Rotunno et al. 2009; Green and Zhang 2015; Ito et al. 2017; Wu et al. 2019). Since LES models parameterize only the small-scale non-energy containing isotropic turbulent eddies, they are often used to examine the performance of mesoscale models. We use output from an LES of the TCBL (referred to as "TC-LES") using the Japan Meteorological Agency's operational regional weather prediction model (JMA-NHM), which is provided by and described in Ito et al. (2017), to compare with the results of our more coarsely resolved CM1 simulations. LES requires a sufficiently small grid resolution (~ 100 m) to represent the largest and most energetic features in a turbulent flow. The JMA-NHM is a fully compressible, non-hydrostatic model and was integrated on a f-plane at 10°N over a horizontal domain size of 2000 km x 2000 km with doubly periodic boundary conditions. Like TC-Param/NonParam, TC-LES was also initiated with an analytic vortex ($U_{t,max}$ = 15 m/s; RMW = 50 km) in a conditionally unstable atmosphere prescribed by a mean tropical sounding (Jordan 1958) and a constant SST set to $27°C$ (300 K) ocean surface. An important distinction between TC-Param/NonParam and TC-LES is that the latter used two consecutive configurations to integrate the model equations: (1) P (mesoscale model for turbulence) run for 120 hrs with a horizontal grid spacing of 2 km, followed by (2) LES run for 10 hrs with a horizontal grid spacing of 100m. The TKE scheme (Deardorff 1980) was used for sub-grid scale parameterization for both P and LES modes and the three-ice single-moment bulk scheme (Lin et al. 1983) was used to parameterize cloud microphysics. Ito et al. (2017) found that the very close to the surface, the simulated TCBL contained strong coherent features that were more or less aligned with the mean tangential flow and identified them as roll vortices (their Figure 4). It will be shown that both TC-Param and TC-NonParam are able to marginally resolve the coherent roll vortices despite a coarser resolution of 500 m; however their characteristics are significantly different than those observed by Ito et al. (2017). From a PV standpoint, further increasing the grid resolution may not necessarily be useful as it is known to contaminate PV by virtue of aliasing and subgrid effects (Bodner and Fox-Kemper 2020).

3. Results and Discussions

a. TC Evolution and Mean Flow Characteristics

The two CM1-simulated TCs exhibit similar intensification rates until Day 8 as shown in Figure 1. Thereafter, TC-Param intensifies more rapidly than TC-NonParam and attains a minimum sea-level pressure (MSLP) and maximum tangential wind speed ($U_{t,max}$) of 967 hPa and 61 m/s respectively at the end of Day 10. At the same time, TC-NonParam has an MSLP and $U_{t,max}$ of about 985 hPa and 48 m/s respectively. Furthermore, TC-Param is a larger storm with an RMW of 16 km and an outer size (R_o) of about 195 km whereas TC-NonParam has an RMW and R_o of 13.5 km and 180 km respectively. Here, R_o is identified as the radius where the azimuthally averaged tangential winds fall to 10% of $U_{t,max}$. The results are consistent with Chavas et al. (2017) in that the central pressure deficit (ΔP) increases with both $U_{t,max}$ and R_o, i.e. $\Delta P \approx F(U_{t,max}, \frac{1}{2} f R_o)$. For further analysis, we focus on the 12 hr period starting at T = 199 hrs due to diverging intensification rates of TC-Param and TC-NonParam during this time. Additionally, we have analyzed ~1 hr of TC-LES model outputs for further comparison. Note that TC-LES may be considered in a quasi-steady state with both its MSLP and $U_{t,max}$ only slightly changing during this time (Figure 1).

The normalized mean wind profiles for three TCs at different radial locations ($R^* = 1, 2, 3$ where $R^* = R/RMW$) are shown in Figure 2. TC-NonParam and TC-LES exhibit strong inflection points in both the mean radial (U_r) and tangential (U_t) winds. The inflection point is the location of maximum vertical shear in the mean wind. It is interesting to note the similarities between TC-NonParam and TC-LES normalized profiles given the Coriolis parameters differ by an order of magnitude. The magnitude of the vertical wind shear is indicative of the strength of the instability that drives the generation of roll vortices. In particular, the primary energy source for roll vortices is the shear production by radial winds ($\overline{u_r w} \partial U_r / \partial z$) where u_r and w are the perturbation radial and vertical winds respectively (Gao and Ginis 2014). The largest radial wind shear for $R^* = 1$ is found in TC-NonParam at a height of 125m. Similar values are found in TC-LES at 195 m whereas TC-Param has a very weak radial wind shear at a height of 325 m. In addition, TC-LES has the deepest shear layer (i.e. height where vertical shear becomes zero), which favors the formation of large roll vortices (Gao and Ginis 2018). One may therefore expect largest and/or most energetic

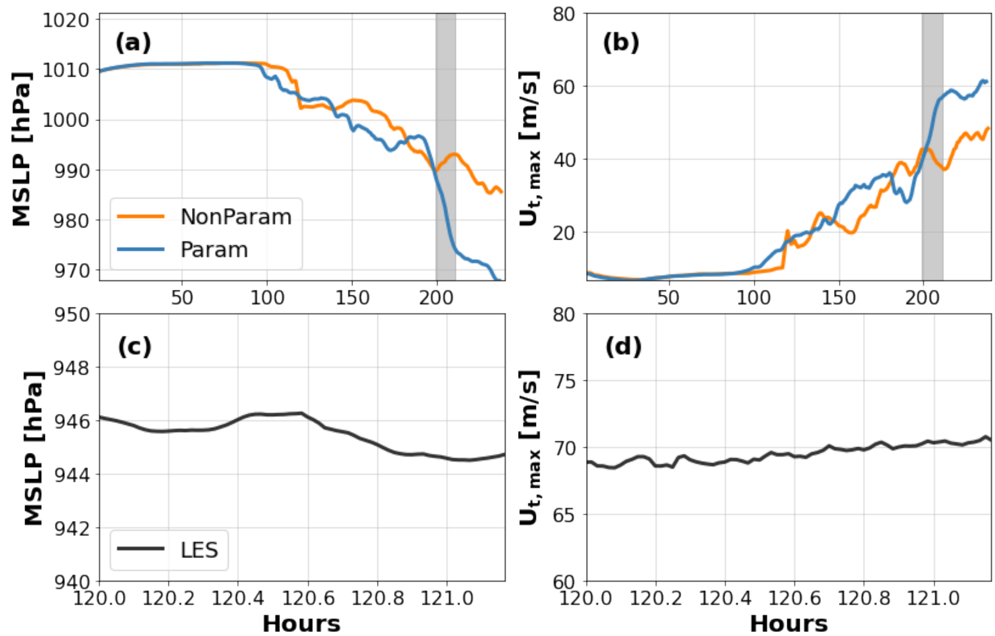

FIG. 1. Time evolution of TC intensity using MSLP (a,c) and U_{max} (b,d) for TC-NonParam and TC-Param (a,b) and TC-LES (c,d) respectively. The shaded region indicates 12 hrs starting at T=199 hr during which TC-Param and TC-NonParam exhibit different rates of intensification.

roll vortices in TC-LES since they can extract kinetic energy from the instability. However, it will be shown in the next few sections that the roll vortices occur more frequently in TC-NonParam and their spatial scales are largest in TC-Param in spite of the weaker vertical shear.

b. Axisymmetric PV structure

The radius-height distribution of the azimuthally averaged dry (θ), virtual (θ_v) and equivalent potential (θ_e) temperatures and the corresponding potential vorticities (PV, PV_v and PV_e) in TC-Param is shown in Figure 3. The PVs are computed at each point using the full 3D fields and are then averaged azimuthally. The axisymmetric structure of PV remains largely unchanged even if computed using azimuthally averaged fields. In all three TCs, the moisture-laden TCBL is characterized by a positive stratification in θ and θ_v and negative stratification in θ_e (Jordan 1958; Dunion 2011) indicating conditional instability to vertical displacements. This instability is fueled by the latent heat fluxes from the surface (Drennan et al. 2007). In addition, unlike its dry counterpart, the total entropy depicted by θ_e has a mid-tropospheric minimum (~4 km) caused

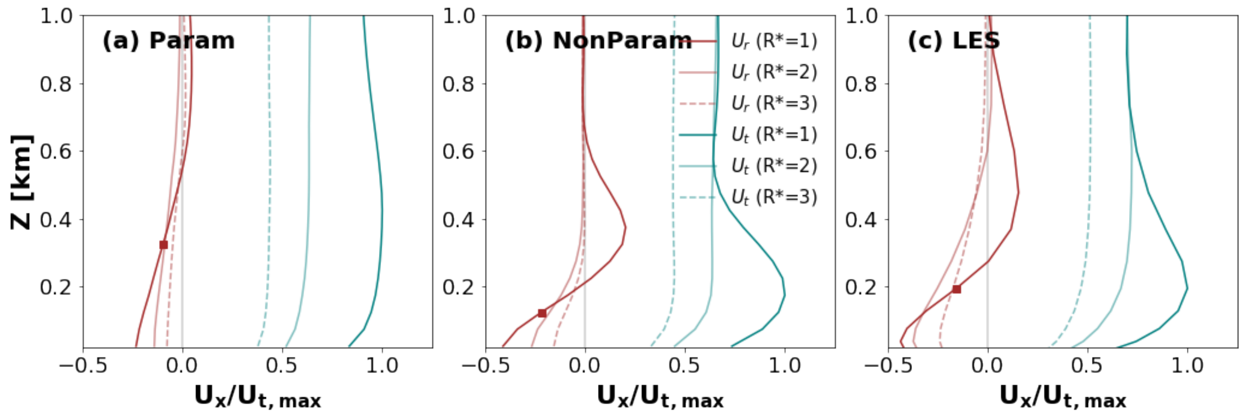

FIG. 2. Vertical profiles of mean radial (x = r; red) and mean tangential (x = t; blue) winds normalized by maximum tangential wind at different radii for (a) TC-Param and (b) TC-NonParam at T=200 hr and (c) TC-LES at T = 120.5 hr. The red squares indicate the inflection points in the radial wind profile. The tangential inflection points lie very close to the surface [lowest model level] and are not shown here.

by competing effects of increasing liquid water entropy and decreasing water content with height (Mrowiec et al. 2011). Consequently, PV and PV_v are positive almost everywhere whereas PV_e is characterized by large negative values inside the TCBL. High magnitudes (10-50 PVU) of PV and PV_v observed inside the eye can be attributed to the large values of vertical vorticity combined with the strong (positive) stratification. However, θ_e is weakly stratified in the eye indicating that the total entropy here is well mixed. PV_e in the eye is an order of magnitude less than PV and PV_v. It should be noted that PV and PV_v are qualitatively and quantitatively very similar largely due to the small effect of moist variables on θ_v computation. θ_e, on the other hand, includes an exponential function of the total water mixing ratio, which amplifies the effect of moist variables.

The axisymmetric PV_e distribution inside the TCBL (0-1 km) reveals several key features. Figures 4 and 5 show the formation and radially outward propagation of a narrow layer of high magnitude negative PV_e [$\mathbf{O}$ (10 PVU)], hereafter referred to as the "Potential Vorticity Minimum Layer" or the "PVML". The PVML is a product of high (negative) vertical stratification in θ_e and high (positive) planetary vorticity (f) and is unique to PV_e distribution. Both TC-Param and TC-NonParam exhibit the PVML in the TCBL, implying its robustness to the parameterization scheme used. However, the parameterization scheme affects the local dynamic and thermodynamic profiles, which can locally

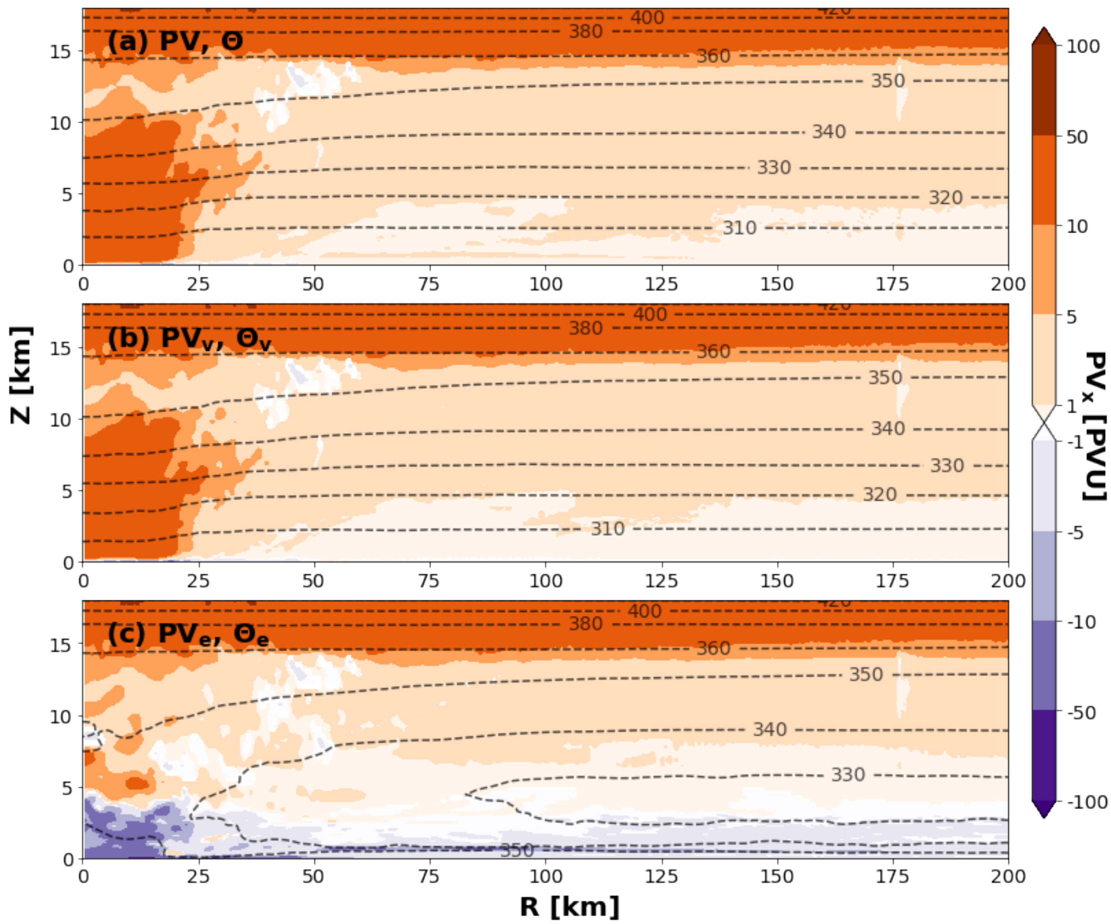

FIG. 3. Azimuthally averaged radial-vertical distribution of θ, θ_v and θ_e (in K) in black dashed contours and the corresponding potential vorticities PV, PV_v and PV_e (in PVU) in shading for TC-Param at t = 200 hr.

impact the intensity and location of the PVML and will be discussed in further sections. Following Haynes and McIntyre (1987), PV_e cannot be transported across isentropic surfaces, hence the only source for the PVML is the region where the isentropes meet the surface, i.e. inside the eye as well as outer radii (R* < 4). Near the surface, PV_e has been shown to be modified by frictional and diabatic processes (Thomas 2005). For both TC-Param and TC-NonParam, the surface processes generate highly negative PV_e, which is then either mixed inside the eye, giving it its strongly negative character, or is advected radially outward along the isentropes as shown in Figures 4 and 5.

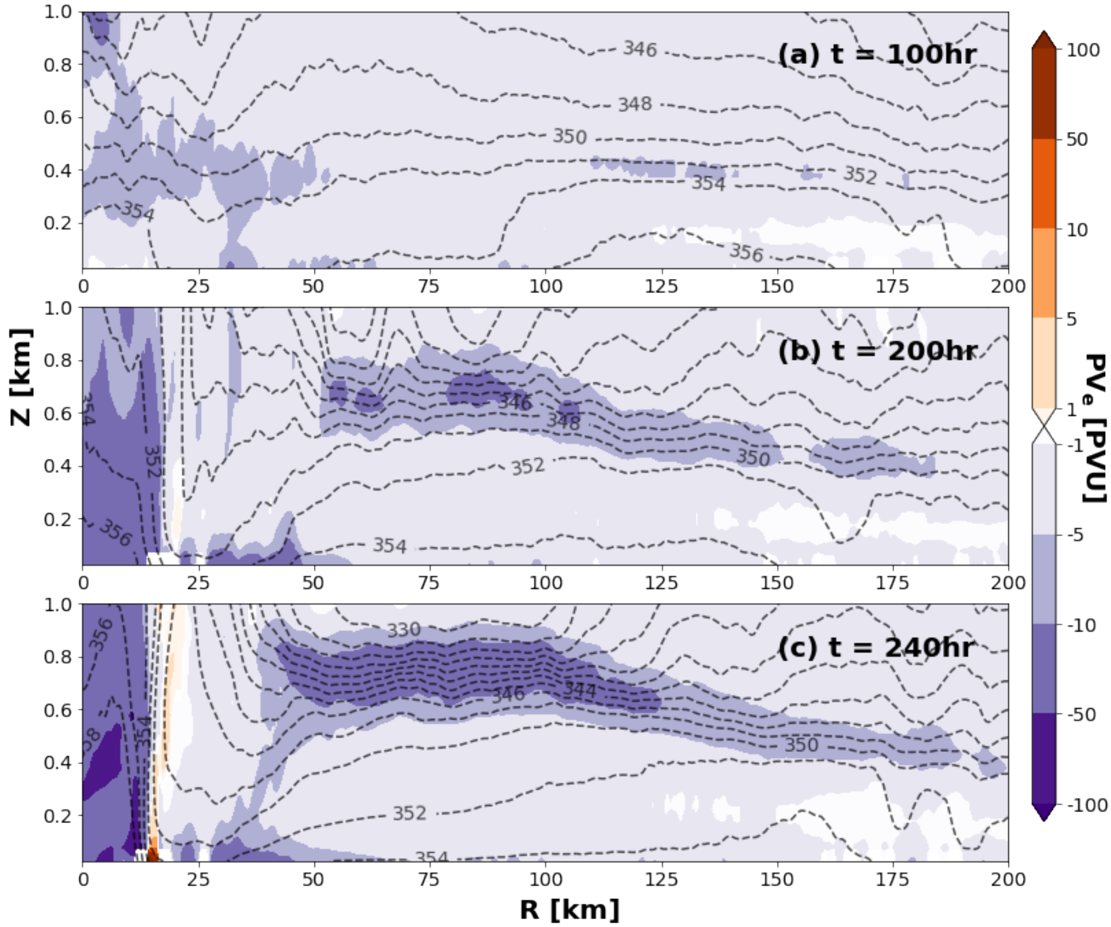

FIG. 4. Azimuthally averaged radial-vertical distribution of PV_e in TC-Param TCBL at (a) t = 100 hr, (b) t = 200 hr and (c) t = 240 hr.

Figure 6 illustrates the radial-vertical structure of the PVML in all three simulated TCs. The axisymmetric PVML height ($\widetilde{h}_{PVML}$) is computed as the height where the radially averaged PV_e, defined in Eq. 3, attains its minimum value.

$$\widetilde{PV_e} = \frac{\int_{r_i}^{r_o} PV_e r dr d\theta}{\int_{r_i}^{r_o} r dr d\theta} \tag{3}$$

PV_e is averaged between inner radius (r_i) of 50 km and outer radius (r_o) of 100 km since the PVML is coherent at these spatial (radial) scales in both TC-Param and TC-NonParam. $\widetilde{h}_{PVML}$ is found to be ~675 m and ~375 m in TC-Param and TC-NonParam respectively. TC-LES also exhibits a broad PVML located at ~300 m. Its magnitude is smaller compared to the others, in part owing to

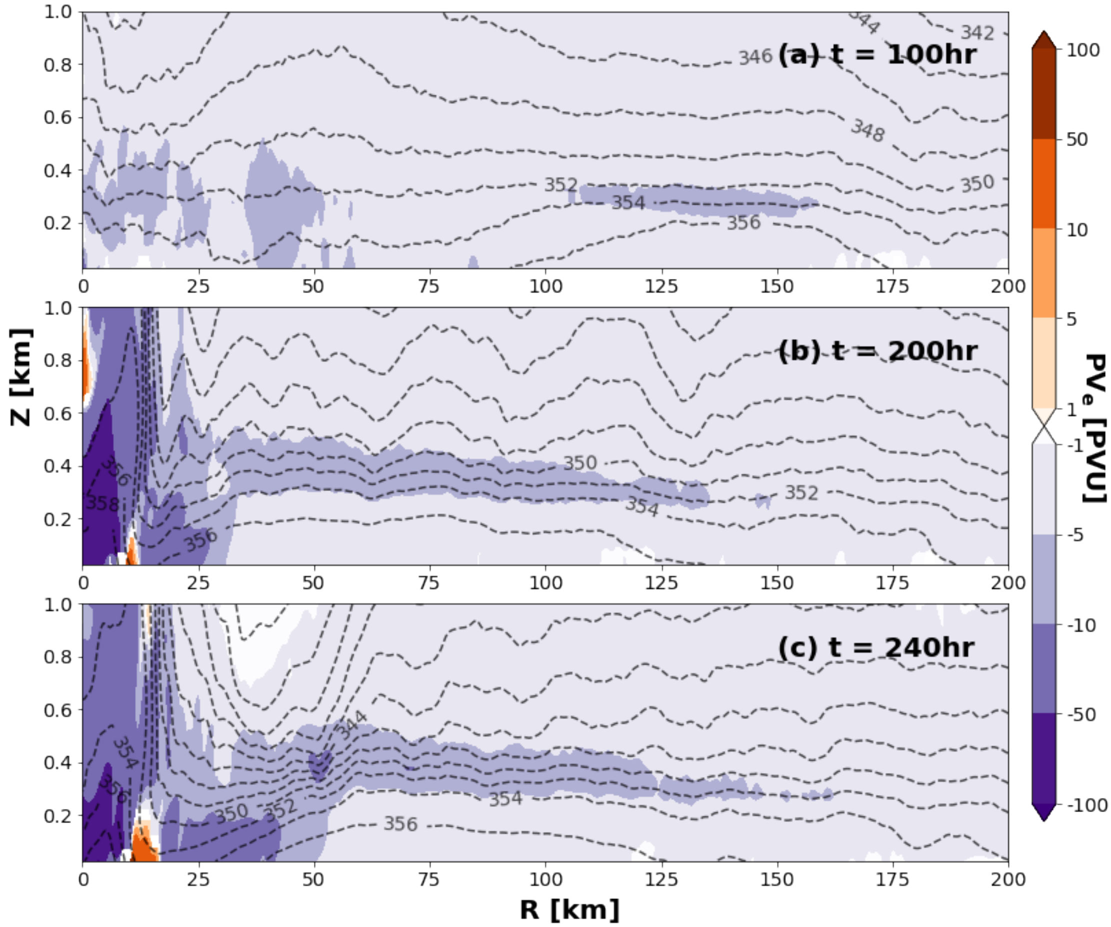

FIG. 5. Same as Figure 4 but for TC-NonParam.

the smaller Coriolis parameter (see supplementary information). The height and magnitude of the PVML decreases with decreasing level of boundary layer parameterization (Param > NonParam > LES). As discussed above, the height of the PVML is closely associated with the height of radial outflow, which is determined by the choice of the parameterization scheme. In TC-LES, the surface processes provide a source of positive PV_e near the broader eye-eyewall region. This is in contrast with the highly negative PV_e found in TC-Param; however TC-NonParam does exhibit similar positive values very close to the eyewall. The positive PV_e in the TC-LES eye is due to the strong stability in this region as indicated by the increasing θ_e with height.

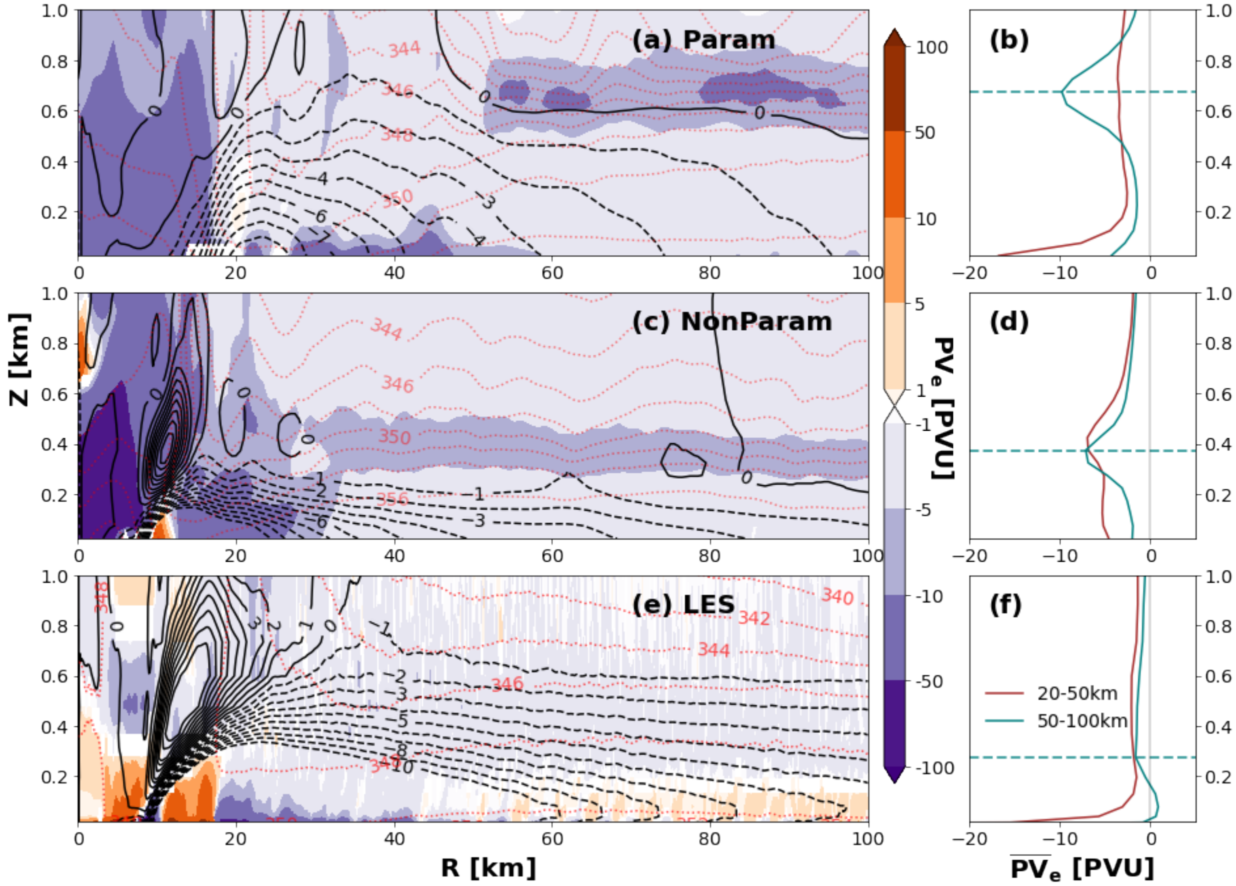

FIG. 6. Azimuthally averaged radial-vertical distribution of PV_e for (a) TC-Param (t=200 hr), (c) TC-NonParam (t=200 hr) and (e) TC-LES (t=120.5 hr). The black dashed and red dotted contours indicate U_r and θ_e respectively. The corresponding vertical profile of $\widetilde{PV_e}$ in radial ranges of 20-50 km (red) and 50-100 km (green) are plotted in b,d,f. The green dashed line indicates $\widetilde{h}_{PVML}$.

c. Asymmetric PV structure

Azimuthally averaged PV_e is primarily dominated by the vertical stratification in θ_e and vertical vorticity. This is supported by the fact that the PVML is observed in both the azimuthally averaged PV_e as well as PV_e computed from azimuthally averaged quantities (see supplementary information). However, the local PV_e inside the TCBL is modulated by both vertical and horizontal gradients. The three-dimensional formulation of PV_e allows us to account for the contributions by local features such as roll vortices that introduce strong radial gradients.

To quantify the effect of roll vortices, the TC domains have been divided into several smaller sub-domains of size 10 km x 10 km x 1 km (see supplementary information) and each sub-domain has been rotated to a local Cartesian coordinate system (x, y, z) such that the y axis is parallel to the direction in which rolls are aligned (typically the mean winds). TC-Param, TC-NonParam and TC-LES are subdivided into 38, 36 and 27 domains respectively. Assuming that roll vortices are quasi-2D features and that the along-roll (y-axis) variations are negligible (Nolan 2005; Gao and Ginis 2014), velocity and other fields are averaged along the y-direction. Eddy velocity fields (u', v', w') are computed by subtracting the velocity components averaged at each height ($\overline{u}, \overline{v}, \overline{w}$). A two-dimensional Q-criterion, also known as the Okubo-Weiss criterion (Okubo 1970; Weiss 1991) is used to identify domains with roll vortices. This criterion defines a vortex as a spatial region where:

$$Q_{2D} \equiv 4\mathrm{Det}(\nabla \mathbf{u}|_{\mathrm{2D}}) - [\mathrm{Tr}(\nabla \mathbf{u}|_{\mathrm{2D}})]^2 > 0 \tag{4}$$

where $\nabla \mathbf{u}|_{2D} = \partial_i u_j (i, j \in \{x, z\})$ is the two-dimensional velocity gradient tensor defined in the across-roll plane. However, $Q_{2D} = 0$ contours have highly irregular shapes owing to the discretization errors introduced while computing velocity gradients. Hence, a positive threshold (5% of $Q_{2D,max}$) is used for each domain to produce smoother vortices that are more aligned with the vortex shape as inferred from the streamlines (Figures 9-11). The 2D-averaged fields in each sub-domain are evaluated every 10 mins for TC-Param/NonParam and every 1 min for TC-LES. An individual time snapshot, referred to as a "scene" (total 72 scenes for each sub-domain over the 12-hr period), that contains at least one vortex with width greater than a threshold ($\lambda_{across} \geq 2.5$ km) is classified as a scene with roll vortices. A threshold of 2.5 km is consistent with observations of coherent eddies in TCBL observations (Guimond et al. 2018; Sroka and Guimond 2021). The local PVML for each scene is identified as the height of the minimum value in the domain-averaged PV_e profile computed in Cartesian coordinates as follows:

$$\overline{\mathrm{PV}}_{\mathrm{e}}(\mathrm{z}) = \frac{\int_{-5\mathrm{km}}^{5\mathrm{km}} \int_{-5\mathrm{km}}^{5\mathrm{km}} \mathrm{PV}_{\mathrm{e}}(\mathrm{x}, \mathrm{y}, \mathrm{z}) \mathrm{dxdy}}{\int_{-5\mathrm{km}}^{5\mathrm{km}} \int_{-5\mathrm{km}}^{5\mathrm{km}} \mathrm{dxdy}}. \tag{5}$$

All three simulations exhibited active roll vortices in at least some scenes (Table 1). TC-NonParam and TC-LES exhibit more roll-rich scenes. However, the roll vortices in TC-Param were found to be larger in size with an average width of 3 km. The average widths of rolls in TC-NonParam and TC-LES were found to be 2.8 km and 0.7 km respectively. In fact, all roll vortices in TC-LES were found to be less than 1.5 km in size. Therefore, the criterion to identify roll-rich scenes in TC-LES was modified to $\lambda_{across} \geq 1.0$ km. The absence of typical sized roll vortices in TC-LES suggests that the radial wind shear or the depth of the shear layer may not have the control on the simulated roll-sizes as suggested by Gao and Ginis (2018). Factors such as horizontal resolution as well as the Coriolis parameter may be important in determining the horizontal and vertical scales of roll vortices and will be examined in further studies.

Roll vortices can interact with the local PVML and subsequently impact its height (h_{PVML}) as shown in Figure 7a. This interaction is possible due to the collocation of the roll-centers and the PVML and is only seen in TC-Param. It is also evident that in the absence of roll vortices, the local PVML can attain heights greater than that of the axisymmetric PVML (Figure 7b). This indicates that the roll vortices modulate the height of the PVML in TC-Param. In TC-NonParam and TC-LES, the roll vortices and the PVML are not collocated and the roll-centers are farther away from the surface than the PVML (Figures 7c,e). As previously noted, the roll vortices in TC-NonParam and TC-LES are smaller in size in addition to being located higher than the PVML. This may explain why the roll vortices in these simulations do not seem to interact with the PVML or modulate the h_{PVML}. This is further shown in Figure 8, where the PVML in TC-NonParam and TC-LES is located at similar heights regardless of the presence or absence of roll vortices. On the contrary, the roll-dominated regions in TC-Param exhibit a lower PVML (625 m) than the roll-deficient regions (675 m). Since the PVML is dominated by the high vertical stratification in θ_e, the difference in h_{PVML} in TC-Param appears entirely due to the difference in θ_e structure (Figure 8c,d). The roll vortices change the thermodynamic structure in the TCBL, through their action on the isentropes, thereby modulating the PVML.

The modulation of h_{PVML} by the roll vortices in TC-Param is further demonstrated in Figure 9a. Since PV_e is a dynamical tracer, changes in its value indicate changes in the nearby flow. As the roll vortices propagate through the domain, the periodic eddy motions around them cause h_{PVML} to fluctuate about an average height of ~400 m. In addition, the roll vortices tend to make

TABLE 1. Number of scenes in each category for different TCs.

	With Rolls ($\lambda_{across} \geq \lambda_o$)	Without Rolls
Param (λ_o = 2.5 km)	332	2404
NonParam (λ_o = 2.5 km)	706	1886
LES (λ_o = 1.0 km)	566	1351

the isentropes more widely spaced causing PV_e dilution. This results in a PVML with a lower magnitude than that in a roll-deficient domain (Figure 9b,d). Without the action of roll vortices, the PVML is considerably stable (less variability) at an average height of ~600 m (Figure 9c). As previously discussed, this mechanism is not significant for TC-NonParam and TC-LES. This is evident in Figure 10 where the roll vortices are either too small or located too far (vertically) to impact h_{PVML} in a meaningful way. It should be noted that several scenes in TC-LES (for example Figure 11a) do exhibit some roll-induced lowering of the local h_{PVML}, however, their impact on the overall h_{PVML} is very small. It is also very challenging to quantify this effect in TC-LES because the large uncertainties in the values of PV_e make it hard to locate the PVML.

d. Comparison with TCBL height scales

Roll characteristics such as the wavelength, height and the growth rate are intricately tied to the dynamical topography (h_{TCBL}) of the TCBL (Nolan 2005; Gao and Ginis 2014). Gao and Ginis (2018) showed that regions with higher h_{TCBL} favor rolls with larger vertical and horizontal extents due to their ability to extract more kinetic energy from the shear layer. Several characteristic height scales have been used to represent h_{TCBL} in models, including determining the mixed layer depth based on potential temperatures (Anthes 1978; Zeng et al. 2004) and dynamic definitions that include the height of maximum winds (Bryan and Rotunno 2009), inflow layer (Smith et al. 2009) and more recently, helicity (Ma and Bao 2016). Both numerical and observational studies have shown considerable separation between these definitions (Zhang et al. 2011; Nolan et al. 2009b). Since small-scale dynamical processes in the TCBL, such as roll vortices, can modulate h_{PVML} via their effects on local thermodynamic structure, we suggest that the diagnosed h_{PVML} can be a useful proxy of the local h_{TCBL}, and it has the desirable property of dependence on a materially conserved variable.

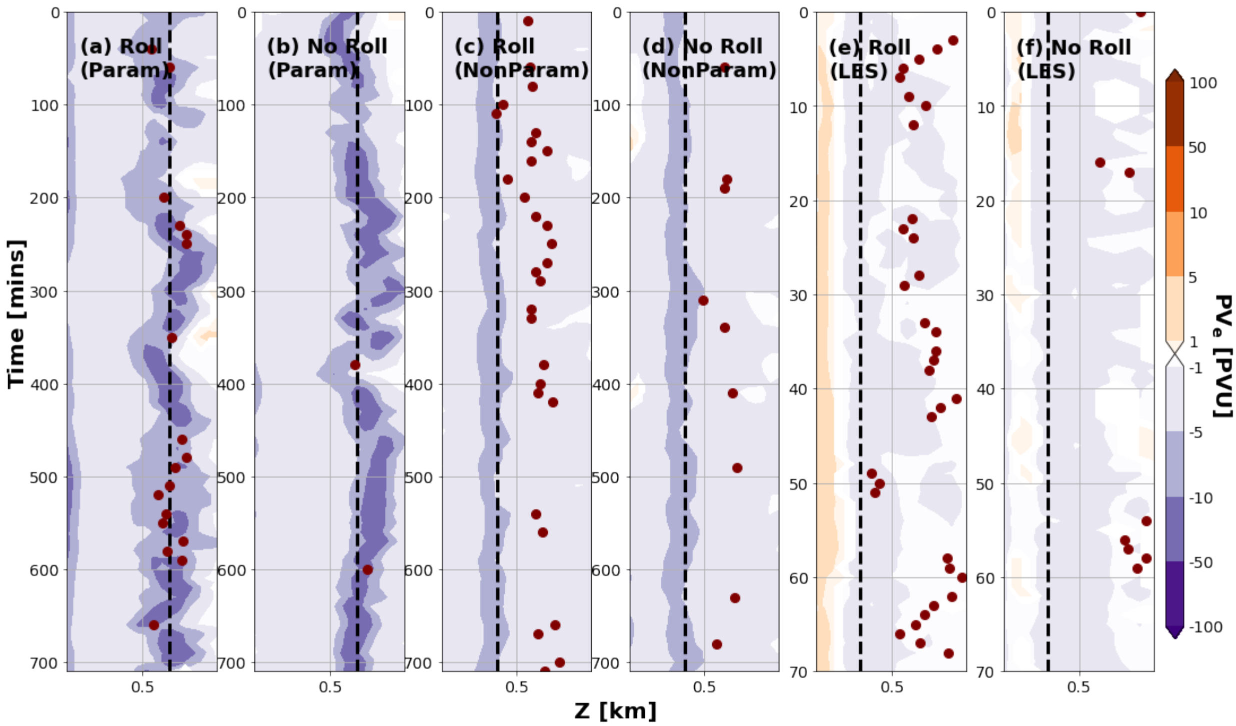

FIG. 7. Time-height variation of PV_e in a (a,b) TC-NonParam, (c,d) TC-Param and (e,f) TC-LES domain with the highest number of roll-rich scenes (a,c,e) and with the lowest number of roll-rich scenes (b,d,f). The red dots indicate the average height of rolls (i.e. vortices with λ_{across} > 2.5 km in TC-Param/NonParam and λ_{across} > 1.0 km in TC-LES), if present. The black dashed lines indicate the height of the axisymmetric PVML (see text). Note that the range for y-axis (time-axis) for TC-Param/NonParam is 0-700 mins while it is 0-70 mins for TC-LES.

Figure 12-14 illustrate the different h_{TCBL} representations including h_{PVML} for TC-Param, TC-NonParam and TC-LES respectively. The elevated values of different h_{TCBL} near the spiral bands in all the simulations indicate that the TCBL is deeper for highly convective regions where the boundary layer air is erupting into the flow above (Smith and Thomsen 2010). As expected, the regions between the spiral bands have low values of h_{TCBL}, due to the entrainment of dry and cool air into the TCBL by convective downdrafts. In TC-Param, h_{PVML} is closer to the thermodynamical definitions: h_{ML1} [$\theta_v - \theta_{v,s}$ > 0.5 K/km; Anthes (1978) and h_{ML2} [$\frac{\partial\theta}{\partial z}$ > 3 K/km; Zeng et al. (2004)] while in TC-LES it closely tracks the dynamical definition: h_{Ri} [height at which the Richardson number attains its critical value (R_{ic}); Hong et al. (2006)]. The PVML in TC-NonParam lies in between the thermodynamical and dynamical h_{TCBL}. This

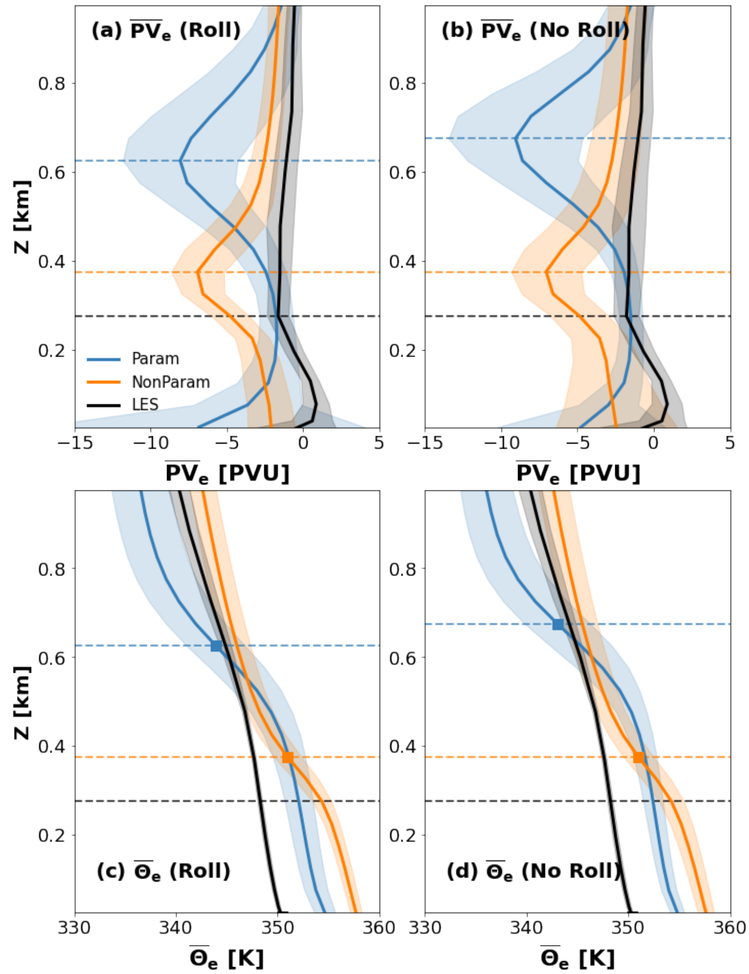

FIG. 8. Vertical profile of (a,b) PV_e and (c,d) θ_e averaged over all domains (a,c) with rolls and (b,d) without rolls over 12 hr (1 hr) period for TC-Param/NonParam (TC-LES). The shaded region indicates 1 standard deviation from the domain-average. The dotted lines indicate the corresponding h_{PVML} and the squares indicate the height of maximum gradient in θ_e. The location of maximum θ_e gradient for TC-LES is very close to the surface and is therefore not shown here.

suggests that both thermodynamic and dynamic processes can control h_{PVML} and their interplay in the different simulations is further discussed. In addition, the PVML lies above the inflow layer ($h_{PVML} > h_{INF}$) in TC-Param and TC-NonParam whereas it lies inside the inflow layer ($h_{PVML} < h_{INF}$) in TC-LES. Here, h_{INF} is identified as the height where inflow reaches 10% of its peak value in the TCBL (Smith et al. 2009; Zhang et al. 2011). This emphasizes the fact that the choice of parameterization, along with additional factors such as different Coriolis parameter

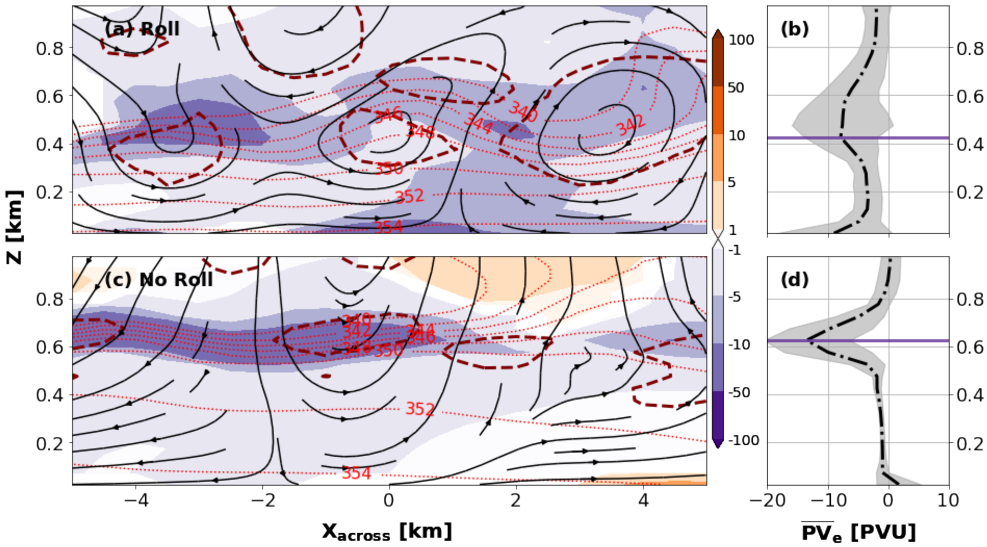

Fig. 9. Radial-vertical cross-section of PV_e (shaded) across the roll axis (x) for TC-Param in a single scene (a) with roll and (c) without roll. The black lines indicate the streamlines computed using eddy-winds (u',w') and the red dotted lines indicate the θ_e contours. Contours of the Q_{2D} threshold value (domain dependent) are marked in maroon dashed lines indicating all vortices. All fields are averaged in the y-direction (i.e. along roll axis). The corresponding vertical profile of domain-averaged PV_e is shown in panels b and d with horizontal purple line indicating the local h_{PVML}.

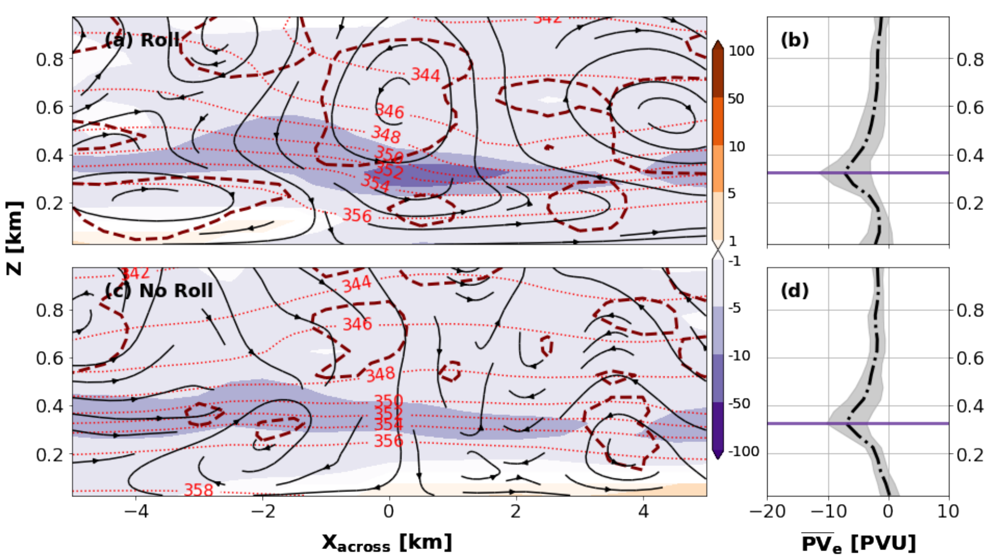

Fig. 10. Same as Figure 9 but for TC-NonParam.

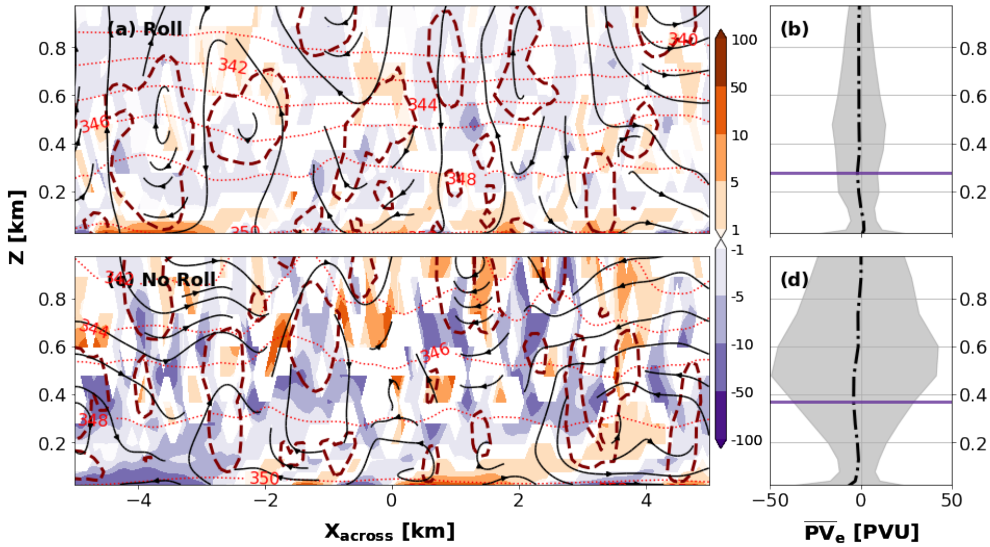

FIG. 11. Same as Figure 9 but for TC-LES.

and horizontal resolution may also play a role in determining the location of PVML.

TC-Param shows little separation between the different definitions of h_{TCBL} (Figure 12, 15a) except h_{Ri}. The turbulence model in all three simulations caps the turbulence at h_{Ri}, i.e. the height at which the Richardson number attains its critical value (R_{ic}) (Hong et al. 2006). Since h_{Ri} starts to notably diverge from other definitions at larger radii, the Richardson number method may not adequately represent h_{TCBL} in TC-Param. The PVML is dominated by the vertical stratification in θ_e (Figure 8) and therefore h_{PVML} may be viewed as a purely thermodynamic definition. This would be consistent with the fact that h_{PVML} is very similar to the mixed layer depths (h_{ML1}, h_{ML2}) in TC-Param. However, it has also been shown for the same simulation that dynamical processes such as roll vortices can change the vertical stratification (in θ_e) inside the TCBL and consequently impact the h_{PVML}.

In TC-NonParam and TC-LES, the mixed layer depths are much higher than h_{PVML} (Figure 13-14, 15b-c) indicating that there is a greater dynamical control on h_{PVML}. In TC-NonParam and TC-LES, the pathway for roll vortices to control h_{PVML} is non-existent due to the large separation between the roll centers and the PVML. This, however, does not preclude other dynamical influences on h_{PVML}. This is clearly evident in the close matching of h_{PVML} with the dynamical definitions

(Figure 13-14, 15b-c). The high correlation between h_{PVML} and h_{Ri} suggests that h_{PVML} in a non-parameterized TCBL is strongly correlated to the height where small-scale turbulence is active. It remains to be seen which of the two dynamical pathways, either through coherent processes such as roll vortices or via small-scale turbulence, controls the thermodynamic structure and therefore the PVML in real TCs. To this end, the foregoing analysis will be extended to simulations of typical TCBLs that can realistically capture small-scale processes (including roll vortices) and compared with dropsonde observations in future work.

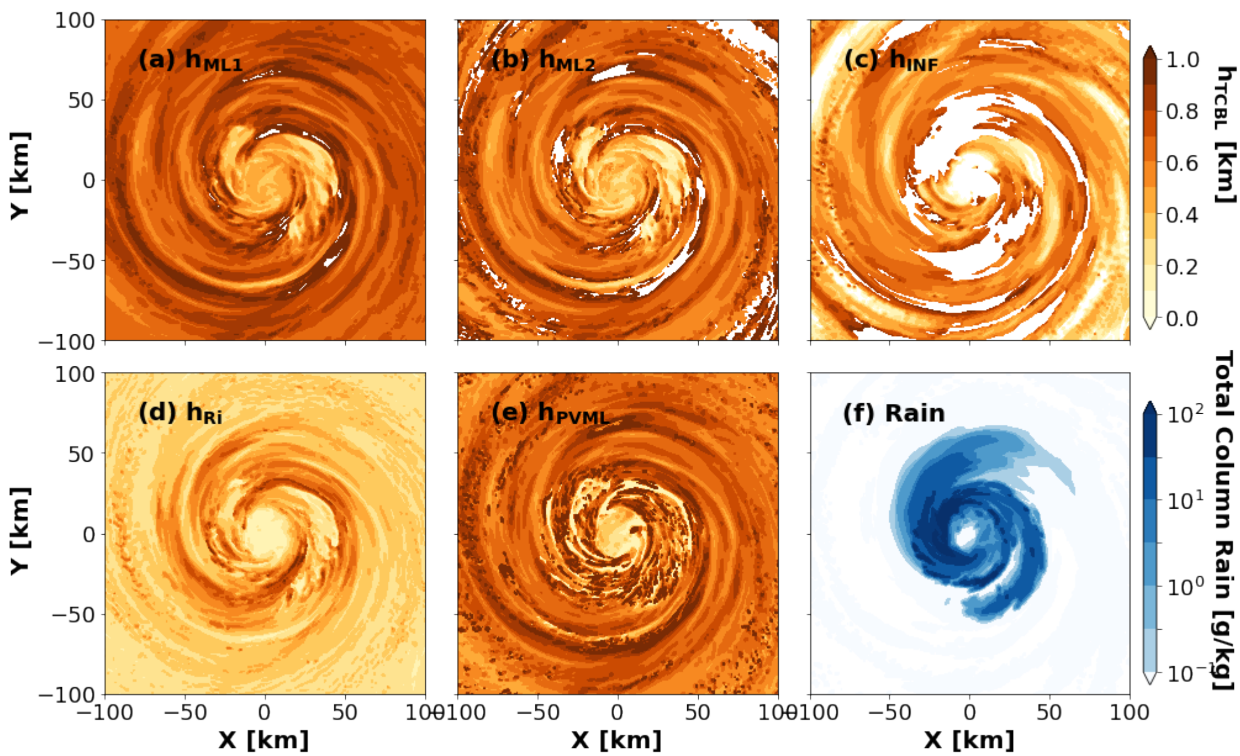

FIG. 12. Characteristic TCBL height scales (h_{TCBL}) for TC-Param at t=199 hr: (a) h_{ML1}, (b) h_{ML2}, (c) h_{INF}, (d) h_{Ri} and (e) h_{PVML}.

4. Conclusions

Our current understanding of the TCBL is limited by the number of observations in this region, and a majority of the h_{TCBL} observational studies assume an axisymmetric structure (Abarca et al. 2015). Three-dimensional observations and numerical studies show that substantial asymmetric structure exists in the TCBL (Kepert 2006a,b; Shapiro 1983; Zhang et al. 2013). We have

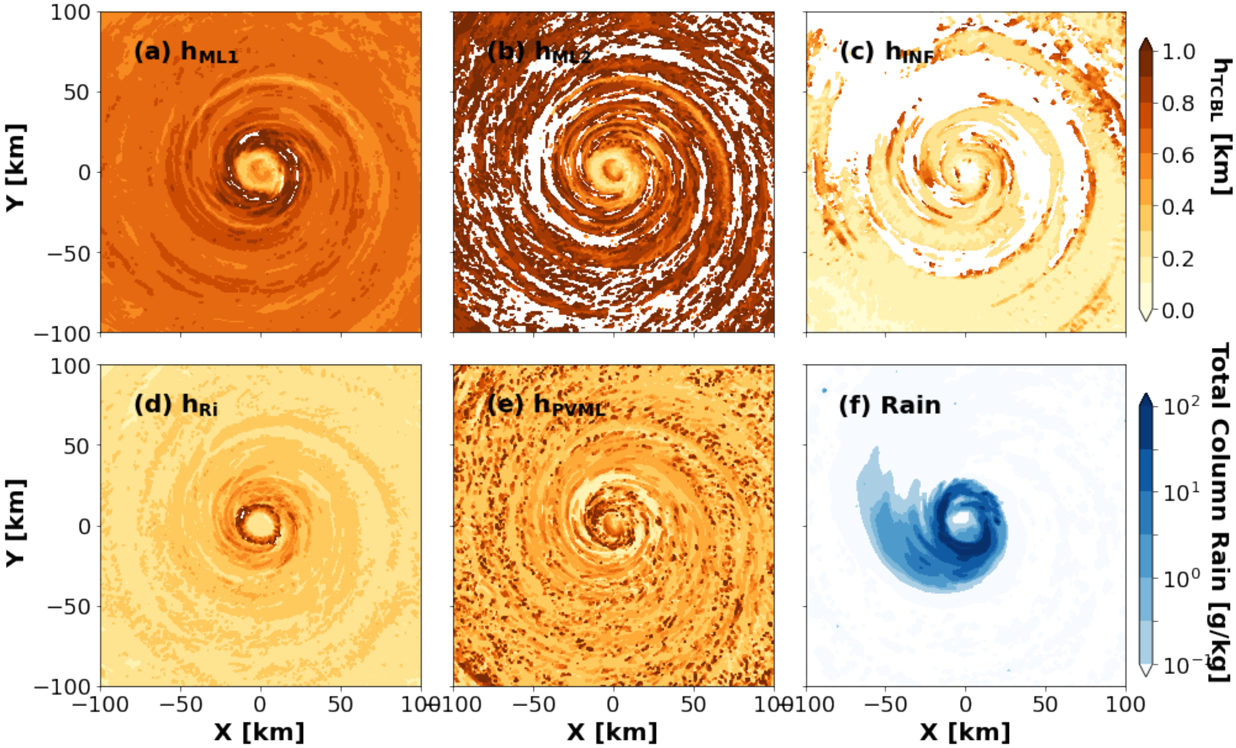

FIG. 13. Same as Figure 12 but for TC-NonParam at t=199 hr.

presented results from two 3D compressible non-hydrostatic simulations of the tropical cyclone boundary layer and investigated the asymmetric structure and small-scale coherent features using the MPV (PV_e) framework. While TC-Param was simulated using a mesoscale model that parameterizes all turbulence, only the sub-grid turbulence was parameterized in TC-NonParam. Using results from a similar LES of the TCBL at a higher resolution (Ito et al. 2017), we showed that a coarser horizontal grid spacing (500 m) for TC-Param/NonParam may be sufficient to marginally represent the small-scale structures likely to correspond to roll vortices.

The TCBL in all three TCs is uniquely characterized as a region of negative PV_e (O(10 PVU) for TC-Param/NonParam and O(1 PVU) for TC-LES) since θ_e is negatively stratified outside the eyewall, indicating moist conditional instability fueled by the latent enthalpy fluxes from the ocean surface. The axisymmetric distribution of PV_e indicates a distinct thin layer of high magnitude PV_e (negative, O(10 PVU)) embedded in the TCBL. The PVML was found to exist in all three simulations, but with varying heights and magnitude. h_{PVML} is shown to be a better proxy for TCBL height compared to other definitions because it combines information about the local wind

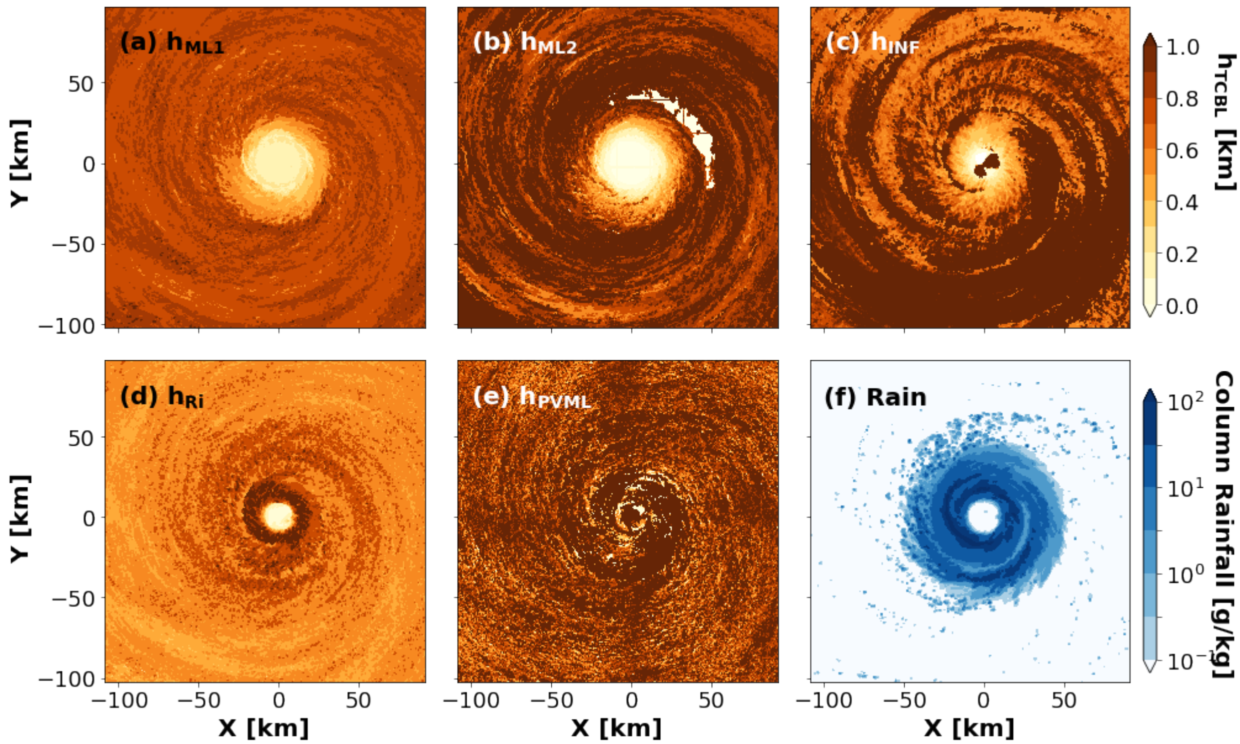

FIG. 14. Same as Figure 12 but for TC-LES at t=120.5 hr.

and thermal structures using a materially conserved variable. Another important property that sets h_{PVML} apart is that it can respond to local flow anomalies such as those created by roll vortices. We find that roll vortices are ubiquitous in the simulated TCBL, regardless of the presence of a boundary layer scheme. However, the characteristics of the roll vortices differ across model schemes and the differing characteristics determine whether or not they interact with the PVML and regulate h_{PVML}. Lastly, we find that an azimuthally averaged field of locally calculated 3D PV_e can be closely estimated by using azimuthally averaged wind and thermodynamic components to define PV_e, except very close to the eyewall. This has an interesting implication for observing the azimuthally averaged PV_e structure of real tropical cyclones: a field of dropsondes that are spatially distributed while close in time could potentially yield a meaningful estimate of the instantaneous azimuthally averaged PV_e structure of a TC. This will be attempted in future work.

Prediction of intense winds in the TCBL still remains one of the major limitations of the current numerical models, partly due to the over-simplification of TCBL contribution via turbulent parameterizations. The parameterization schemes that are developed for moderate wind conditions often

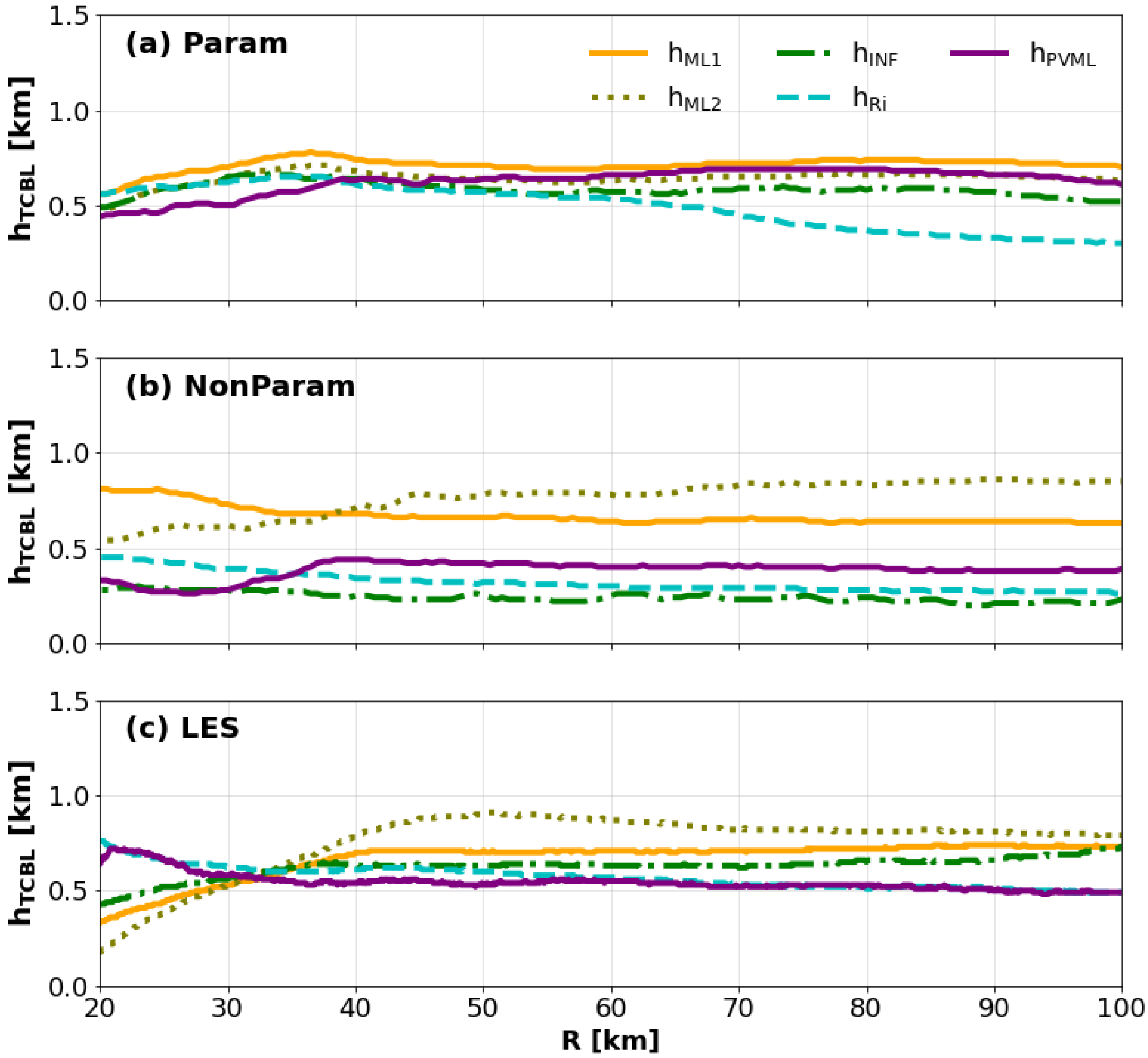

FIG. 15. Radial distribution of azimuthally averaged h_{TCBL} represented by different height scales averaged over 12 hrs for (a) TC-Param and (b) TC-NonParam and over 1 hr for (c) TC-LES.

cannot accurately account for the fluxes induced by small-scale processes such as roll vortices (Foster 2005; Gao and Ginis 2014, 2016). The PVML can provide a useful link between the small-scale processes and the large-scale dynamics in highly-resolved models. An important caveat of this study is that we are not able to separate the impacts of the order-of-magnitude-higher Coriolis parameter in TC-Param and Non-Param compared to TC-LES from their differing grid spacings, due to computational expense. However, the finding of a PVML (albeit one of lower magnitude in TC-LES) gives us confidence that this feature should be robust to model differences. The sensitivity of the results to the different subgrid turbulence schemes remains. In particular, subgrid turbulence schemes that can accurately capture the roll characteristics including the associated counter-gradient fluxes will be examined in future studies.

Acknowledgments. The authors thank David Nolan, Hao Fu, Leif Thomas, Jacob Wenegrat and Abigail Bodner for the insightful discussions and suggestions. The authors are also grateful to Junshi Ito at Meteorological Research Institute, Japan as well as the Japan Meteorological Agency for sharing their high-resolution simulations with us. We acknowledge high-performance computing support provided by Stanford Research Computing Center and thank Stanford University for funding this study.

Data availability statement. The datasets on which this paper is based are too large to be publicly archived with available resources and can be made available upon request by the authors. The codes and corresponding figures used to support this study are available at https://tinyurl.com/2e4cek7m. The output of TC-LES is from the high resolution simulation described in Ito et al. (2017) and provided by Junshi Ito.

References

Abarca, S. F., M. T. Montgomery, and J. C. McWilliams, 2015: The azimuthally averaged boundary layer structure of a numerically simulated major hurricane: BOUNDARY LAYER OF A MAJOR HURRICANE. *Journal of Advances in Modeling Earth Systems*, **7 (3)**, 1207–1219, https://doi.org/10.1002/2015MS000457, URL http://doi.wiley.com/10.1002/2015MS000457.

Anthes, R. A., 1978: The Height of the Planetary Boundary Layer and the Production of Circulation in a Sea Breeze Model. *Journal of the Atmospheric Sciences*, **35 (7)**, 1231–1239, https://doi.org/10.1175/1520-0469(1978)035<1231:THOTPB>2.0.CO;2, URL https://journals.ametsoc.org/view/journals/atsc/35/7/1520-0469_1978_035_1231_thotpb_2_0_co_2.xml, publisher: American Meteorological Society Section: Journal of the Atmospheric Sciences.

Baldauf, M., A. Seifert, J. Förstner, D. Majewski, M. Raschendorfer, and T. Reinhardt, 2011: Operational Convective-Scale Numerical Weather Prediction with the COSMO Model: Description and Sensitivities. *Monthly Weather Review*, **139 (12)**, 3887–3905, https://doi.org/10.1175/MWR-D-10-05013.1, URL https://journals.ametsoc.org/mwr/article/139/12/3887/107618/Operational-Convective-Scale-Numerical-Weather, publisher: American Meteorological Society.

Bennetts, D. A., and B. J. Hoskins, 1979: Conditional symmetric instability - a possible explanation for frontal rainbands. *Quarterly Journal of the Royal Meteorological Society*, **105 (446)**, 945–962, https://doi.org/10.1002/qj.49710544615, URL https://rmets.onlinelibrary.wiley.com/doi/abs/10.1002/qj.49710544615.

Bodner, A. S., and B. Fox-Kemper, 2020: A Breakdown in Potential Vorticity Estimation Delineates the Submesoscale-to-Turbulence Boundary in Large Eddy Simulations. *Journal of Advances in Modeling Earth Systems*, **12 (10)**, e2020MS002 049, https://doi.org/10.1029/2020MS002049, URL https://onlinelibrary.wiley.com/doi/abs/10.1029/2020MS002049, _eprint: https://onlinelibrary.wiley.com/doi/pdf/10.1029/2020MS002049.

Braun, S. A., J. A. Sippel, and D. S. Nolan, 2011: The Impact of Dry Midlevel Air on Hurricane Intensity in Idealized Simulations with No Mean Flow. *Journal of the Atmospheric Sciences*, **69 (1)**, 236–257, https://doi.org/10.1175/JAS-D-10-05007.1, URL https://journals.ametsoc.org/doi/full/10.1175/JAS-D-10-05007.1, publisher: American Meteorological Society.

Braun, S. A., and W.-K. Tao, 2000: Sensitivity of High-Resolution Simulations of Hurricane Bob (1991) to Planetary Boundary Layer Parameterizations. *Monthly Weather Review*, **128 (12)**, 3941–3961, https://doi.org/10.1175/1520-0493(2000)129<3941:SOHRSO>2.0.CO;2, URL https://journals.ametsoc.org/mwr/article/128/12/3941/104455/Sensitivity-of-High-Resolution-Simulations-of, publisher: American Meteorological Society.

Bryan, G. H., 2011: Effects of Surface Exchange Coefficients and Turbulence Length Scales on the Intensity and Structure of Numerically Simulated Hurricanes. *Monthly Weather Review*, **140 (4)**, 1125–1143, https://doi.org/10.1175/MWR-D-11-00231.1, URL https://journals.ametsoc.org/doi/full/10.1175/MWR-D-11-00231.1.

Bryan, G. H., and J. M. Fritsch, 2002: A Benchmark Simulation for Moist Nonhydrostatic Numerical Models. *Monthly Weather Review*, **130 (12)**, 2917–2928, https://doi.org/10.1175/1520-0493(2002)130<2917:ABSFMN>2.0.CO;2, URL https://journals.ametsoc.org/doi/full/10.1175/1520-0493%282002%29130%3C2917%3AABSFMN%3E2.0.CO%3B2.

Bryan, G. H., and R. Rotunno, 2009: The Maximum Intensity of Tropical Cyclones in Axisymmetric Numerical Model Simulations. *Monthly Weather Review*, **137 (6)**, 1770–1789, https://doi.org/10.1175/2008MWR2709.1, URL https://journals.ametsoc.org/doi/full/10.1175/2008MWR2709.1.

Bu, Y. P., R. G. Fovell, and K. L. Corbosiero, 2017: The Influences of Boundary Layer Mixing and Cloud-Radiative Forcing on Tropical Cyclone Size. *Journal of the Atmospheric Sciences*, **74 (4)**, 1273–1292, https://doi.org/10.1175/JAS-D-16-0231.1, URL https://journals.ametsoc.org/doi/10.1175/JAS-D-16-0231.1.

Cao, Z., and H.-R. Cho, 1995: Generation of Moist Potential Vorticity in Extratropical Cyclones. *Journal of the Atmospheric Sciences*, **52 (18)**, 3263–3282, https://doi.org/10.1175/1520-0469(1995)052<3263:GOMPVI>2.0.CO;2, URL https://journals.ametsoc.org/jas/article/52/18/3263/23742/Generation-of-Moist-Potential-Vorticity-in, publisher: American Meteorological Society.

Chagnon, J. M., and S. L. Gray, 2009: Horizontal potential vorticity dipoles on the convective storm scale. *Quarterly Journal of the Royal Meteorological Society*, **135 (643)**, 1392–1408, https://doi.org/10.1002/qj.468, URL https://rmets.onlinelibrary.wiley.com/doi/abs/10.1002/qj.468, _eprint: https://rmets.onlinelibrary.wiley.com/doi/pdf/10.1002/qj.468.

Chavas, D. R., K. A. Reed, and J. A. Knaff, 2017: Physical understanding of the tropical cyclone wind-pressure relationship. *Nature Communications*, **8 (1)**, 1360, https://doi.org/10.1038/s41467-017-01546-9, URL https://www.nature.com/articles/s41467-017-01546-9, number: 1 Publisher: Nature Publishing Group.

Cione, J. J., E. A. Kalina, J. A. Zhang, and E. W. Uhlhorn, 2013: Observations of Air–Sea Interaction and Intensity Change in Hurricanes. *Monthly Weather Review*, **141 (7)**, 2368–2382, https://doi.org/10.1175/MWR-D-12-00070.1, URL https://journals.ametsoc.org/mwr/article/141/7/2368/71869/Observations-of-Air-Sea-Interaction-and-Intensity, publisher: American Meteorological Society.

Cione, J. J., and Coauthors, 2020: Eye of the Storm: Observing Hurricanes with a Small Unmanned Aircraft System. *Bulletin of the American Meteorological Society*, **101 (2)**, E186–E205, https://doi.org/10.1175/BAMS-D-19-0169.1, URL https://journals.ametsoc.org/bams/article/101/2/E186/345056/Eye-of-the-Storm-Observing-Hurricanes-with-a-Small, publisher: American Meteorological Society.

Clarke, S. J., S. L. Gray, and N. M. Roberts, 2019: Downstream influence of mesoscale convective systems. Part 1: influence on forecast evolution. *Quarterly Journal of the Royal Meteorological Society*, **145 (724)**, 2933–2952, https://doi.org/10.1002/qj.3593, URL https://rmets.onlinelibrary.wiley.com/doi/abs/10.1002/qj.3593, _eprint: https://rmets.onlinelibrary.wiley.com/doi/pdf/10.1002/qj.3593.

Davis, C. A., and K. A. Emanuel, 1991: Potential Vorticity Diagnostics of Cyclogenesis. *Monthly Weather Review*, **119 (8)**, 1929–1953, https://doi.org/10.1175/1520-0493(1991)119<1929:PVDOC>2.0.CO;2, URL https://journals.ametsoc.org/mwr/article/119/8/1929/64469/Potential-Vorticity-Diagnostics-of-Cyclogenesis, publisher: American Meteorological Society.

Deardorff, J. W., 1980: Stratocumulus-capped mixed layers derived from a three-dimensional model. *Boundary-Layer Meteorology*, **18 (4)**, 495–527, https://doi.org/10.1007/BF00119502, URL https://doi.org/10.1007/BF00119502.

Drennan, W. M., J. A. Zhang, J. R. French, C. McCormick, and P. G. Black, 2007: Turbulent Fluxes in the Hurricane Boundary Layer. Part II: Latent Heat Flux. *Journal of the Atmospheric Sciences*, **64 (4)**, 1103–1115, https://doi.org/10.1175/JAS3889.1, URL https://journals.ametsoc.org/doi/10.1175/JAS3889.1.

Dunion, J. P., 2011: Rewriting the Climatology of the Tropical North Atlantic and Caribbean Sea Atmosphere. *Journal of Climate*, **24 (3)**, 893–908, https://doi.org/10.1175/2010JCLI3496.1, URL https://journals.ametsoc.org/view/journals/clim/24/3/2010jcli3496.1.xml, publisher: American Meteorological Society Section: Journal of Climate.

Ellis, R., and S. Businger, 2010: Helical circulations in the typhoon boundary layer. *Journal of Geophysical Research: Atmospheres*, **115 (D6)**, https://doi.org/10.1029/2009JD011819, URL https://agupubs.onlinelibrary.wiley.com/doi/abs/10.1029/2009JD011819, _eprint: https://agupubs.onlinelibrary.wiley.com/doi/pdf/10.1029/2009JD011819.

Emanuel, K. A., 1979: Inertial Instability and Mesoscale Convective Systems. Part I: Linear Theory of Inertial Instability in Rotating Viscous Fluids. *Journal of the Atmospheric Sciences*, **36 (12)**, 2425–2449, https://doi.org/10.1175/1520-0469(1979)

036<2425:IIAMCS>2.0.CO;2, URL https://journals.ametsoc.org/jas/article/36/12/2425/19742/Inertial-Instability-and-Mesoscale-Convective, publisher: American Meteorological Society.

Emanuel, K. A., 1986: An Air-Sea Interaction Theory for Tropical Cyclones. Part I: Steady-State Maintenance. *Journal of the Atmospheric Sciences*, **43 (6)**, 585–605, https://doi.org/10.1175/1520-0469(1986)043<0585:AASITF>2.0.CO;2, URL https://doi.org/10.1175/1520-0469(1986)043<0585:AASITF>2.0.CO;2.

Emanuel, K. A., 1994: *Atmospheric Convection*. Oxford University Press (New York).

Emanuel, K. A., 1995: Sensitivity of Tropical Cyclones to Surface Exchange Coefficients and a Revised Steady-State Model incorporating Eye Dynamics. *Journal of the Atmospheric Sciences*, **52 (22)**, 3969–3976, https://doi.org/10.1175/1520-0469(1995)052<3969:SOTCTS>2.0.CO;2, URL https://journals.ametsoc.org/jas/article/52/22/3969/23938/Sensitivity-of-Tropical-Cyclones-to-Surface, publisher: American Meteorological Society.

Fierro, A. O., R. F. Rogers, F. D. Marks, and D. S. Nolan, 2009: The Impact of Horizontal Grid Spacing on the Microphysical and Kinematic Structures of Strong Tropical Cyclones Simulated with the WRF-ARW Model. *Monthly Weather Review*, **137 (11)**, 3717–3743, https://doi.org/10.1175/2009MWR2946.1, URL https://journals.ametsoc.org/mwr/article/137/11/3717/70634/The-Impact-of-Horizontal-Grid-Spacing-on-the, publisher: American Meteorological Society.

Foster, R., 2013: Signature of Large Aspect Ratio Roll Vortices in Synthetic Aperture Radar Images of Tropical Cyclones. *Oceanography*, **26 (2)**, https://doi.org/10.5670/oceanog.2013.31, URL https://tos.org/oceanography/article/signature-of-large-aspect-ratio-roll-vortices-in-synthetic-aperture-radar-i.

Foster, R. C., 2005: Why Rolls are Prevalent in the Hurricane Boundary Layer. *Journal of the Atmospheric Sciences*, **62 (8)**, 2647–2661, https://doi.org/10.1175/JAS3475.1, URL https://journals.ametsoc.org/doi/10.1175/JAS3475.1.

Gao, K., and I. Ginis, 2014: On the Generation of Roll Vortices due to the Inflection Point Instability of the Hurricane Boundary Layer Flow. *Journal of the Atmospheric Sciences*, **71 (11)**, 4292–4307, https://doi.org/10.1175/JAS-D-13-0362.1, URL https://journals.ametsoc.org/jas/article/

71/11/4292/27547/On-the-Generation-of-Roll-Vortices-due-to-the, publisher: American Meteorological Society.

Gao, K., and I. Ginis, 2016: On the Equilibrium-State Roll Vortices and Their Effects in the Hurricane Boundary Layer. *Journal of the Atmospheric Sciences*, **73 (3)**, 1205–1222, https://doi.org/10.1175/JAS-D-15-0089.1, URL https://journals.ametsoc.org/jas/article/73/3/1205/342493/On-the-Equilibrium-State-Roll-Vortices-and-Their, publisher: American Meteorological Society.

Gao, K., and I. Ginis, 2018: On the Characteristics of Linear-Phase Roll Vortices under a Moving Hurricane Boundary Layer. *Journal of the Atmospheric Sciences*, **75 (8)**, 2589–2598, https://doi.org/10.1175/JAS-D-17-0363.1, URL https://journals.ametsoc.org/jas/article/75/8/2589/68983/On-the-Characteristics-of-Linear-Phase-Roll, publisher: American Meteorological Society.

Gao, K., I. Ginis, J. D. Doyle, and Y. Jin, 2017: Effect of Boundary Layer Roll Vortices on the Development of an Axisymmetric Tropical Cyclone. *Journal of the Atmospheric Sciences*, **74 (9)**, 2737–2759, https://doi.org/10.1175/JAS-D-16-0222.1, URL https://journals.ametsoc.org/doi/full/10.1175/JAS-D-16-0222.1.

Gao, S., X. Wang, and Y. Zhou, 2004: Generation of generalized moist potential vorticity in a frictionless and moist adiabatic flow. *Geophysical Research Letters*, **31 (12)**, https://doi.org/10.1029/2003GL019152, URL https://agupubs.onlinelibrary.wiley.com/doi/abs/10.1029/2003GL019152, _eprint: https://agupubs.onlinelibrary.wiley.com/doi/pdf/10.1029/2003GL019152.

Gentry, M. S., and G. M. Lackmann, 2010: Sensitivity of Simulated Tropical Cyclone Structure and Intensity to Horizontal Resolution. *Monthly Weather Review*, **138 (3)**, 688–704, https://doi.org/10.1175/2009MWR2976.1, URL https://journals.ametsoc.org/mwr/article/138/3/688/71074/Sensitivity-of-Simulated-Tropical-Cyclone, publisher: American Meteorological Society.

Gopalakrishnan, S. G., F. Marks, J. A. Zhang, X. Zhang, J.-W. Bao, and V. Tallapragada, 2013: A Study of the Impacts of Vertical Diffusion on the Structure and Intensity of the Tropical Cyclones

Using the High-Resolution HWRF System. *Journal of the Atmospheric Sciences*, **70 (2)**, 524–541, https://doi.org/10.1175/JAS-D-11-0340.1, URL https://journals.ametsoc.org/jas/article/70/2/524/43401/A-Study-of-the-Impacts-of-Vertical-Diffusion-on, publisher: American Meteorological Society.

Green, B. W., and F. Zhang, 2015: Idealized Large-Eddy Simulations of a Tropical Cyclone–like Boundary Layer. *Journal of the Atmospheric Sciences*, **72 (5)**, 1743–1764, https://doi.org/10.1175/JAS-D-14-0244.1, URL https://journals.ametsoc.org/doi/full/10.1175/JAS-D-14-0244.1.

Guimond, S. R., J. A. Zhang, J. W. Sapp, and S. J. Frasier, 2018: Coherent Turbulence in the Boundary Layer of Hurricane Rita (2005) during an Eyewall Replacement Cycle. *Journal of the Atmospheric Sciences*, **75 (9)**, 3071–3093, https://doi.org/10.1175/JAS-D-17-0347.1, URL https://journals.ametsoc.org/jas/article/75/9/3071/69054/Coherent-Turbulence-in-the-Boundary-Layer-of, publisher: American Meteorological Society.

Harvey, B., J. Methven, C. Sanchez, and A. Schäfler, 2020: Diabatic generation of negative potential vorticity and its impact on the North Atlantic jet stream. *Quarterly Journal of the Royal Meteorological Society*, **146 (728)**, 1477–1497, https://doi.org/10.1002/qj.3747, URL https://rmets.onlinelibrary.wiley.com/doi/abs/10.1002/qj.3747, _eprint: https://rmets.onlinelibrary.wiley.com/doi/pdf/10.1002/qj.3747.

Haynes, P. H., and M. E. McIntyre, 1987: On the Evolution of Vorticity and Potential Vorticity in the Presence of Diabatic Heating and Frictional or Other Forces. *Journal of the Atmospheric Sciences*, **44 (5)**, 828–841, https://doi.org/10.1175/1520-0469(1987)044<0828:OTEOVA>2.0.CO;2, URL https://journals.ametsoc.org/doi/10.1175/1520-0469%281987%29044%3C0828%3AOTEOVA%3E2.0.CO%3B2, publisher: American Meteorological Society.

Hong, S.-Y., Y. Noh, and J. Dudhia, 2006: A New Vertical Diffusion Package with an Explicit Treatment of Entrainment Processes. *Monthly Weather Review*, **134 (9)**, 2318–2341, https://doi.org/10.1175/MWR3199.1, URL https://journals.ametsoc.org/doi/full/10.1175/MWR3199.1.

Ito, J., T. Oizumi, and H. Niino, 2017: Near-surface coherent structures explored by large eddy simulation of entire tropical cyclones. *Scientific Reports*, **7 (1)**, 3798, https://doi.org/10.1038/s41598-017-03848-w, URL http://www.nature.com/articles/s41598-017-03848-w.

Jordan, C. L., 1958: MEAN SOUNDINGS FOR THE WEST INDIES AREA. *Journal of the Atmospheric Sciences*, **15 (1)**, 91–97, https://doi.org/10.1175/1520-0469(1958)015<0091:MSFTWI>2.0.CO;2, URL https://journals.ametsoc.org/view/journals/atsc/15/1/1520-0469_1958_015_0091_msftwi_2_0_co_2.xml, publisher: American Meteorological Society Section: Journal of the Atmospheric Sciences.

Kepert, J. D., 2006a: Observed Boundary Layer Wind Structure and Balance in the Hurricane Core. Part I: Hurricane Georges. *Journal of the Atmospheric Sciences*, **63 (9)**, 2169–2193, https://doi.org/10.1175/JAS3745.1, URL https://journals.ametsoc.org/view/journals/atsc/63/9/jas3745.1.xml, publisher: American Meteorological Society Section: Journal of the Atmospheric Sciences.

Kepert, J. D., 2006b: Observed Boundary Layer Wind Structure and Balance in the Hurricane Core. Part II: Hurricane Mitch. *Journal of the Atmospheric Sciences*, **63 (9)**, 2194–2211, https://doi.org/10.1175/JAS3746.1, URL https://journals.ametsoc.org/view/journals/atsc/63/9/jas3746.1.xml, publisher: American Meteorological Society Section: Journal of the Atmospheric Sciences.

Kepert, J. D., 2011: Choosing a Boundary Layer Parameterization for Tropical Cyclone Modeling. *Monthly Weather Review*, **140 (5)**, 1427–1445, https://doi.org/10.1175/MWR-D-11-00217.1, URL https://journals.ametsoc.org/doi/full/10.1175/MWR-D-11-00217.1.

Khairoutdinov, M., and K. Emanuel, 2013: Rotating radiative-convective equilibrium simulated by a cloud-resolving model: ROTATING RCE. *Journal of Advances in Modeling Earth Systems*, **5 (4)**, 816–825, https://doi.org/10.1002/2013MS000253, URL http://doi.wiley.com/10.1002/2013MS000253.

Kilroy, G., R. K. Smith, and M. T. Montgomery, 2016: Why Do Model Tropical Cyclones Grow Progressively in Size and Decay in Intensity after Reaching Maturity? *Journal of the Atmospheric Sciences*, **73 (2)**, 487–503, https://doi.org/10.1175/JAS-D-15-0157.1, URL https://journals.ametsoc.org/jas/article/73/2/487/27791/Why-Do-Model-Tropical-Cyclones-Grow-Progressively, publisher: American Meteorological Society.

Liang, Z., C. Lu, and E. I. Tollerud, 2010: Diagnostic study of generalized moist potential vorticity in a non-uniformly saturated atmosphere with heavy precipitation. *Quarterly Journal of the Royal Meteorological Society*, **136 (650)**, 1275–1288, https://doi.org/10.1002/qj.636, URL https://rmets.onlinelibrary.wiley.com/doi/abs/10.1002/qj.636, _eprint: https://rmets.onlinelibrary.wiley.com/doi/pdf/10.1002/qj.636.

Lin, Y.-L., R. D. Farley, and H. D. Orville, 1983: Bulk Parameterization of the Snow Field in a Cloud Model. *Journal of Climate and Applied Meteorology*, **22 (6)**, 1065–1092, https://doi.org/10.1175/1520-0450(1983)022<1065:BPOTSF>2.0.CO;2, URL https://journals.ametsoc.org/jamc/article/22/6/1065/352507/Bulk-Parameterization-of-the-Snow-Field-in-a-Cloud, publisher: American Meteorological Society.

Lorsolo, S., J. L. Schroeder, P. Dodge, and F. Marks, 2008: An Observational Study of Hurricane Boundary Layer Small-Scale Coherent Structures. *Monthly Weather Review*, **136 (8)**, 2871–2893, https://doi.org/10.1175/2008MWR2273.1, URL https://journals.ametsoc.org/view/journals/mwre/136/8/2008mwr2273.1.xml, publisher: American Meteorological Society Section: Monthly Weather Review.

Ma, L.-M., and X.-W. Bao, 2016: Parametrization of Planetary Boundary-Layer Height with Helicity and Verification with Tropical Cyclone Prediction. *Boundary-Layer Meteorology*, **160 (3)**, 569–593, https://doi.org/10.1007/s10546-016-0156-7, URL https://doi.org/10.1007/s10546-016-0156-7.

Marks, F. D., P. G. Black, M. T. Montgomery, and R. W. Burpee, 2008: Structure of the Eye and Eyewall of Hurricane Hugo (1989). *Monthly Weather Review*, **136 (4)**, 1237–1259, https://doi.org/10.1175/2007MWR2073.1, URL https://journals.ametsoc.org/doi/full/10.1175/2007MWR2073.1.

Marquet, P., 2014: On the definition of a moist-air potential vorticity. *Quarterly Journal of the Royal Meteorological Society*, **140 (680)**, 917–929, https://doi.org/10.1002/qj.2182, URL https://rmets.onlinelibrary.wiley.com/doi/abs/10.1002/qj.2182.

Ming, J., and J. A. Zhang, 2016: Effects of surface flux parameterization on the numerically simulated intensity and structure of Typhoon Morakot (2009). *Advances in Atmospheric Sci-*

ences, **33 (1)**, 58–72, https://doi.org/10.1007/s00376-015-4202-z, URL https://doi.org/10.1007/s00376-015-4202-z.

Molinari, J., S. Skubis, and D. Vollaro, 1995: External Influences on Hurricane Intensity. Part III: Potential Vorticity Structure. *Journal of the Atmospheric Sciences*, **52 (20)**, 3593–3606, https://doi.org/10.1175/1520-0469(1995)052<3593:EIOHIP>2.0.CO;2, URL https://journals.ametsoc.org/doi/abs/10.1175/1520-0469(1995)052%3C3593%3AEIOHIP%3E2.0.CO%3B2.

Montgomery, M. T., and B. F. Farrell, 1993: Tropical Cyclone Formation. *Journal of the Atmospheric Sciences*, **50 (2)**, 285–310, https://doi.org/10.1175/1520-0469(1993)050<0285:TCF>2.0.CO;2, URL https://journals.ametsoc.org/view/journals/atsc/50/2/1520-0469_1993_050_0285_tcf_2_0_co_2.xml, publisher: American Meteorological Society Section: Journal of the Atmospheric Sciences.

Morrison, H., and A. Gettelman, 2008: A New Two-Moment Bulk Stratiform Cloud Microphysics Scheme in the Community Atmosphere Model, Version 3 (CAM3). Part I: Description and Numerical Tests. *Journal of Climate*, **21 (15)**, 3642–3659, https://doi.org/10.1175/2008JCLI2105.1, URL https://journals.ametsoc.org/jcli/article/21/15/3642/32043/A-New-Two-Moment-Bulk-Stratiform-Cloud, publisher: American Meteorological Society.

Morrison, I., S. Businger, F. Marks, P. Dodge, and J. A. Businger, 2005: An Observational Case for the Prevalence of Roll Vortices in the Hurricane Boundary Layer*. *Journal of the Atmospheric Sciences*, **62 (8)**, 2662–2673, https://doi.org/10.1175/JAS3508.1, URL https://journals.ametsoc.org/doi/10.1175/JAS3508.1.

Mrowiec, A. A., S. T. Garner, and O. M. Pauluis, 2011: Axisymmetric Hurricane in a Dry Atmosphere: Theoretical Framework and Numerical Experiments. *Journal of the Atmospheric Sciences*, **68 (8)**, 1607–1619, https://doi.org/10.1175/2011JAS3639.1, URL https://journals.ametsoc.org/jas/article/68/8/1607/27211/Axisymmetric-Hurricane-in-a-Dry-Atmosphere, publisher: American Meteorological Society.

Nolan, D. S., 2005: Instabilities in hurricane-like boundary layers. *Dynamics of Atmospheres and Oceans*, **40 (3)**, 209–236, https://doi.org/10.1016/j.dynatmoce.2005.03.002, URL http://www.sciencedirect.com/science/article/pii/S0377026505000096.

Nolan, D. S., D. P. Stern, and J. A. Zhang, 2009a: Evaluation of Planetary Boundary Layer Parameterizations in Tropical Cyclones by Comparison of In Situ Observations and High-Resolution Simulations of Hurricane Isabel (2003). Part II: Inner-Core Boundary Layer and Eyewall Structure. *Monthly Weather Review*, **137 (11)**, 3675–3698, https://doi.org/10.1175/2009MWR2786.1, URL https://journals.ametsoc.org/mwr/article/137/11/3675/70644/Evaluation-of-Planetary-Boundary-Layer, publisher: American Meteorological Society.

Nolan, D. S., J. A. Zhang, and D. P. Stern, 2009b: Evaluation of Planetary Boundary Layer Parameterizations in Tropical Cyclones by Comparison of In Situ Observations and High-Resolution Simulations of Hurricane Isabel (2003). Part I: Initialization, Maximum Winds, and the Outer-Core Boundary Layer. *Monthly Weather Review*, **137 (11)**, 3651–3674, https://doi.org/10.1175/2009MWR2785.1, URL https://journals.ametsoc.org/mwr/article/137/11/3651/70629/Evaluation-of-Planetary-Boundary-Layer, publisher: American Meteorological Society.

Oertel, A., M. Boettcher, H. Joos, M. Sprenger, and H. Wernli, 2019: Potential vorticity structure of embedded convection in a warm conveyor belt and its relevance for the large-scale dynamics. preprint, Dynamical processes in midlatitudes. https://doi.org/10.5194/wcd-2019-3, URL https://wcd.copernicus.org/preprints/wcd-2019-3/wcd-2019-3.pdf.

Okubo, A., 1970: Horizontal dispersion of floatable particles in the vicinity of velocity singularities such as convergences. *Deep Sea Research and Oceanographic Abstracts*, **17 (3)**, 445–454, https://doi.org/10.1016/0011-7471(70)90059-8, URL https://www.sciencedirect.com/science/article/pii/0011747170900598.

Persing, J., M. T. Montgomery, J. C. McWilliams, and R. K. Smith, 2013: Asymmetric and axisymmetric dynamics of tropical cyclones. *Atmos. Chem. Phys.*, 43.

Rotunno, R., Y. Chen, W. Wang, C. Davis, J. Dudhia, and G. J. Holland, 2009: Large-Eddy Simulation of an Idealized Tropical Cyclone. *Bulletin of the American Meteorological Society*, **90 (12)**, 1783–1788, https://doi.org/10.1175/2009BAMS2884.1, URL https://journals.ametsoc.org/bams/article/90/12/1783/59589/Large-Eddy-Simulation-of-an-Idealized-Tropical, publisher: American Meteorological Society.

Rotunno, R., and K. A. Emanuel, 1987: An Air–Sea Interaction Theory for Tropical Cyclones. Part II: Evolutionary Study Using a Nonhydrostatic Axisymmetric Numerical Model. *Journal of the*

Atmospheric Sciences, **44 (3)**, 542–561, https://doi.org/10.1175/1520-0469(1987)044<0542:AAITFT>2.0.CO;2, URL https://journals.ametsoc.org/doi/abs/10.1175/1520-0469%281987%29044%3C0542%3AAAITFT%3E2.0.CO%3B2.

Schubert, W. H., S. A. Hausman, M. Garcia, K. V. Ooyama, and H.-C. Kuo, 2001: Potential Vorticity in a Moist Atmosphere. *Journal of the Atmospheric Sciences*, **58 (21)**, 3148–3157, https://doi.org/10.1175/1520-0469(2001)058<3148:PVIAMA>2.0.CO;2, URL https://journals.ametsoc.org/doi/full/10.1175/1520-0469%282001%29058%3C3148%3APVIAMA%3E2.0.CO%3B2.

Schubert, W. H., M. T. Montgomery, R. K. Taft, T. A. Guinn, S. R. Fulton, J. P. Kossin, and J. P. Edwards, 1999: Polygonal Eyewalls, Asymmetric Eye Contraction, and Potential Vorticity Mixing in Hurricanes. *Journal of the Atmospheric Sciences*, **56 (9)**, 1197–1223, https://doi.org/10.1175/1520-0469(1999)056<1197:PEAECA>2.0.CO;2, URL https://journals.ametsoc.org/doi/full/10.1175/1520-0469%281999%29056%3C1197%3APEAECA%3E2.0.CO%3B2.

Sessions, S. L., S. Sentić, and D. J. Raymond, 2019: Balanced Dynamics and Moisture Quasi-Equilibrium in DYNAMO Convection. *Journal of the Atmospheric Sciences*, **76 (9)**, 2781–2799, https://doi.org/10.1175/JAS-D-18-0173.1, URL https://journals.ametsoc.org/view/journals/atsc/76/9/jas-d-18-0173.1.xml, publisher: American Meteorological Society Section: Journal of the Atmospheric Sciences.

Shapiro, L. J., 1983: The Asymmetric Boundary layer Flow Under a Translating Hurricane. *Journal of the Atmospheric Sciences*, **40 (8)**, 1984–1998, https://doi.org/10.1175/1520-0469(1983)040<1984:TABLFU>2.0.CO;2, URL http://journals.ametsoc.org/doi/abs/10.1175/1520-0469%281983%29040%3C1984%3ATABLFU%3E2.0.CO%3B2.

Shapiro, L. J., and J. L. Franklin, 1995: Potential Vorticity in Hurricane Gloria. *Monthly Weather Review*, **123 (5)**, 1465–1475, https://doi.org/10.1175/1520-0493(1995)123<1465:PVIHG>2.0.CO;2, URL https://journals.ametsoc.org/view/journals/mwre/123/5/1520-0493_1995_123_1465_pvihg_2_0_co_2.xml, publisher: American Meteorological Society Section: Monthly Weather Review.

Shutts, G., 2017: Idealized numerical simulations of Mesoscale Convective Systems and their implications for forecast error. *Quarterly Journal of the Royal Meteorological Society*, **143 (704)**, 1608–1619, https://doi.org/10.1002/qj.3031, URL https://rmets.onlinelibrary.wiley.com/doi/abs/10.1002/qj.3031, _eprint: https://rmets.onlinelibrary.wiley.com/doi/pdf/10.1002/qj.3031.

Smith, R. K., and M. T. Montgomery, 2015: Toward Clarity on Understanding Tropical Cyclone Intensification. *Journal of the Atmospheric Sciences*, **72 (8)**, 3020–3031, https://doi.org/10.1175/JAS-D-15-0017.1, URL https://doi.org/10.1175/JAS-D-15-0017.1.

Smith, R. K., M. T. Montgomery, and N. Van Sang, 2009: Tropical cyclone spin-up revisited. *Quarterly Journal of the Royal Meteorological Society*, **135 (642)**, 1321–1335, https://doi.org/10.1002/qj.428, URL https://onlinelibrary.wiley.com/doi/abs/10.1002/qj.428, _eprint: https://onlinelibrary.wiley.com/doi/pdf/10.1002/qj.428.

Smith, R. K., and G. L. Thomsen, 2010: Dependence of tropical-cyclone intensification on the boundary-layer representation in a numerical model. *Quarterly Journal of the Royal Meteorological Society*, **136 (652)**, 1671–1685, https://doi.org/10.1002/qj.687, URL https://rmets.onlinelibrary.wiley.com/doi/abs/10.1002/qj.687, _eprint: https://rmets.onlinelibrary.wiley.com/doi/pdf/10.1002/qj.687.

Sroka, S., and S. Guimond, 2021: Organized kinetic energy backscatter in the hurricane boundary layer from radar measurements. *Journal of Fluid Mechanics*, **924**, A21, https://doi.org/10.1017/jfm.2021.632, URL https://www.cambridge.org/core/product/identifier/S0022112021006327/type/journal_article.

Sukhanovskii, A., and E. Popova, 2020: The Importance of Horizontal Rolls in the Rapid Intensification of Tropical Cyclones. *Boundary-Layer Meteorology*, **175 (2)**, 259–276, https://doi.org/10.1007/s10546-020-00503-2, URL https://doi.org/10.1007/s10546-020-00503-2.

Thomas, L. N., 2005: Destruction of Potential Vorticity by Winds. *Journal of Physical Oceanography*, **35 (12)**, 2457–2466, https://doi.org/10.1175/JPO2830.1, URL https://journals.ametsoc.org/doi/full/10.1175/JPO2830.1, publisher: American Meteorological Society.

Thorpe, A. J., 1985: Diagnosis of Balanced Vortex Structure Using Potential Vorticity. *Journal of the Atmospheric Sciences*, **42 (4)**, 397–406, https://doi.org/10.1175/1520-0469(1985)042<0397:DOBVSU>2.0.CO;2, URL https://journals.ametsoc.org/doi/10.1175/1520-0469%281985%29042%3C0397%3ADOBVSU%3E2.0.CO%3B2.

Wang, X., and D.-L. Zhang, 2003: Potential Vorticity Diagnosis of a Simulated Hurricane. Part I: Formulation and Quasi-Balanced Flow. *Journal of the Atmospheric Sciences*, **60 (13)**, 1593–1607, https://doi.org/10.1175/2999.1, URL https://journals.ametsoc.org/doi/full/10.1175/2999.1.

Weijenborg, C., J. M. Chagnon, P. Friederichs, S. L. Gray, and A. Hense, 2017: Coherent evolution of potential vorticity anomalies associated with deep moist convection. *Quarterly Journal of the Royal Meteorological Society*, **143 (704)**, 1254–1267, https://doi.org/10.1002/qj.3000, URL https://rmets.onlinelibrary.wiley.com/doi/abs/10.1002/qj.3000, _eprint: https://rmets.onlinelibrary.wiley.com/doi/pdf/10.1002/qj.3000.

Weiss, J., 1991: The dynamics of enstrophy transfer in two-dimensional hydrodynamics. *Physica D: Nonlinear Phenomena*, **48 (2)**, 273–294, https://doi.org/10.1016/0167-2789(91)90088-Q, URL https://www.sciencedirect.com/science/article/pii/016727899190088Q.

Wetzel, A. N., L. M. Smith, S. N. Stechmann, J. E. Martin, and Y. Zhang, 2020: Potential Vorticity and Balanced and Unbalanced Moisture. *Journal of the Atmospheric Sciences*, https://doi.org/10.1175/JAS-D-19-0311.1, URL https://journals.ametsoc.org/doi/abs/10.1175/JAS-D-19-0311.1, publisher: American Meteorological Society.

Wu, C.-C., and K. A. Emanuel, 1993: Interaction of a Baroclinic Vortex with Background Shear: Application to Hurricane Movement. *Journal of the Atmospheric Sciences*, **50 (1)**, 62–76, https://doi.org/10.1175/1520-0469(1993)050<0062:IOABVW>2.0.CO;2, URL https://journals.ametsoc.org/view/journals/atsc/50/1/1520-0469_1993_050_0062_ioabvw_2_0_co_2.xml, publisher: American Meteorological Society Section: Journal of the Atmospheric Sciences.

Wu, L., Q. Liu, and Y. Li, 2019: Tornado-scale vortices in the tropical cyclone boundary layer: numerical simulation with the WRF–LES framework. *Atmospheric Chemistry and Physics*, **19 (4)**, 2477–2487, https://doi.org/10.5194/acp-19-2477-2019, URL https://www.atmos-chem-phys.net/19/2477/2019/.

Wurman, J., and J. Winslow, 1998: Intense Sub-Kilometer-Scale Boundary Layer Rolls Observed in Hurricane Fran. *Science*, **280 (5363)**, 555–557, https://doi.org/10.1126/science.280.5363.555, URL https://science.sciencemag.org/content/280/5363/555, publisher: American Association for the Advancement of Science Section: Report.

Zeng, X., M. A. Brunke, M. Zhou, C. Fairall, N. A. Bond, and D. H. Lenschow, 2004: Marine Atmospheric Boundary Layer Height over the Eastern Pacific: Data Analysis and Model Evaluation. *Journal of Climate*, **17 (21)**, 4159–4170, https://doi.org/10.1175/JCLI3190.1, URL https://journals.ametsoc.org/view/journals/clim/17/21/jcli3190.1.xml, publisher: American Meteorological Society Section: Journal of Climate.

Zhang, J. A., K. B. Katsaros, P. G. Black, S. Lehner, J. R. French, and W. M. Drennan, 2008: Effects of Roll Vortices on Turbulent Fluxes in the Hurricane Boundary Layer. *Boundary-Layer Meteorology*, **128 (2)**, 173–189, https://doi.org/10.1007/s10546-008-9281-2, URL https://doi.org/10.1007/s10546-008-9281-2.

Zhang, J. A., R. F. Rogers, D. S. Nolan, and F. D. Marks, 2011: On the Characteristic Height Scales of the Hurricane Boundary Layer. *Monthly Weather Review*, **139 (8)**, 2523–2535, https://doi.org/10.1175/MWR-D-10-05017.1, URL https://journals.ametsoc.org/doi/full/10.1175/MWR-D-10-05017.1.

Zhang, J. A., R. F. Rogers, P. D. Reasor, E. W. Uhlhorn, and F. D. Marks, 2013: Asymmetric Hurricane Boundary Layer Structure from Dropsonde Composites in Relation to the Environmental Vertical Wind Shear. *Monthly Weather Review*, **141 (11)**, 3968–3984, https://doi.org/10.1175/MWR-D-12-00335.1, URL https://journals.ametsoc.org/doi/full/10.1175/MWR-D-12-00335.1.

Zhu, P., 2008: Simulation and parameterization of the turbulent transport in the hurricane boundary layer by large eddies. *Journal of Geophysical Research*, **113 (D17)**, D17 104, https://doi.org/10.1029/2007JD009643, URL http://doi.wiley.com/10.1029/2007JD009643.

fw

Supplementary Information

S1. The three-dimensional PV_e is largely dominated by the vertical components due to the large value of absolute vertical vorticity. This is indicated by little to no differences between azimuthally averaged 3D-PV_e and PV_e computed from azimuthally averaged fields as shown in Figures 1(a-c). However, 3D-PV_e may exhibit significant differences from the vertical component over smaller spatial scales.

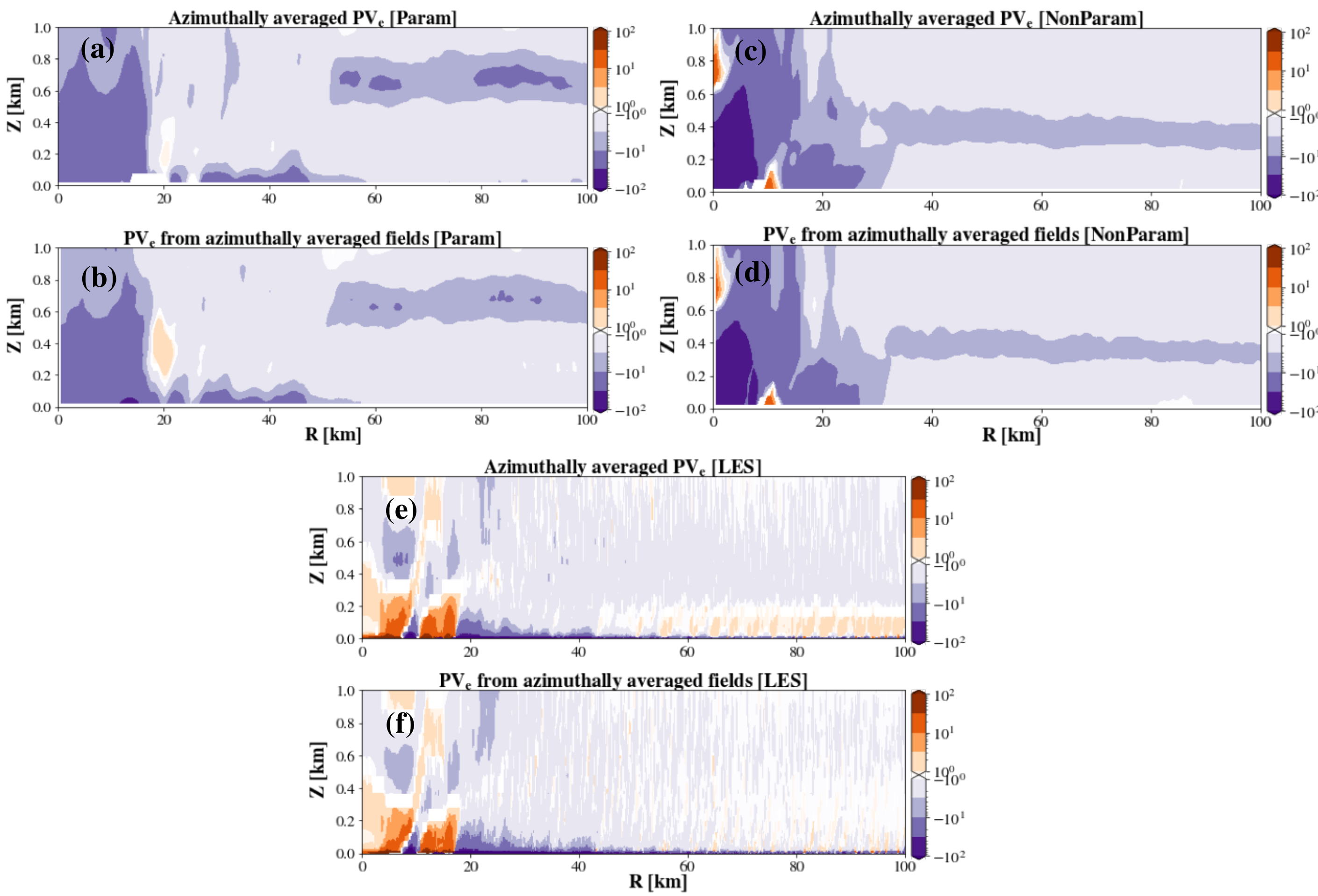

Figure 1. Radial-vertical distribution of PVe in (a-b) TC-Param at t=199 h, (c-d) TC-NonParam at t=199 hr and (e-f) TC-LES at t=120.5 hr.

S2. The high magnitude of the Coriolis parameter results in the high magnitude PVML in TC-Param and TC-NonParam. As shown in Figure 2, incorporating a lower value of f (equal to what is used in TC-LES), results in a low magnitude PVML in TC-NonParam, similar to that observed in TC-LES. For instance, the PVML magnitude in TC-Param is about -10 PVU, if we use the same flow field but substitute the high Coriolis parameter with a typical low value (2.5×10^{-5} s^{-1}):

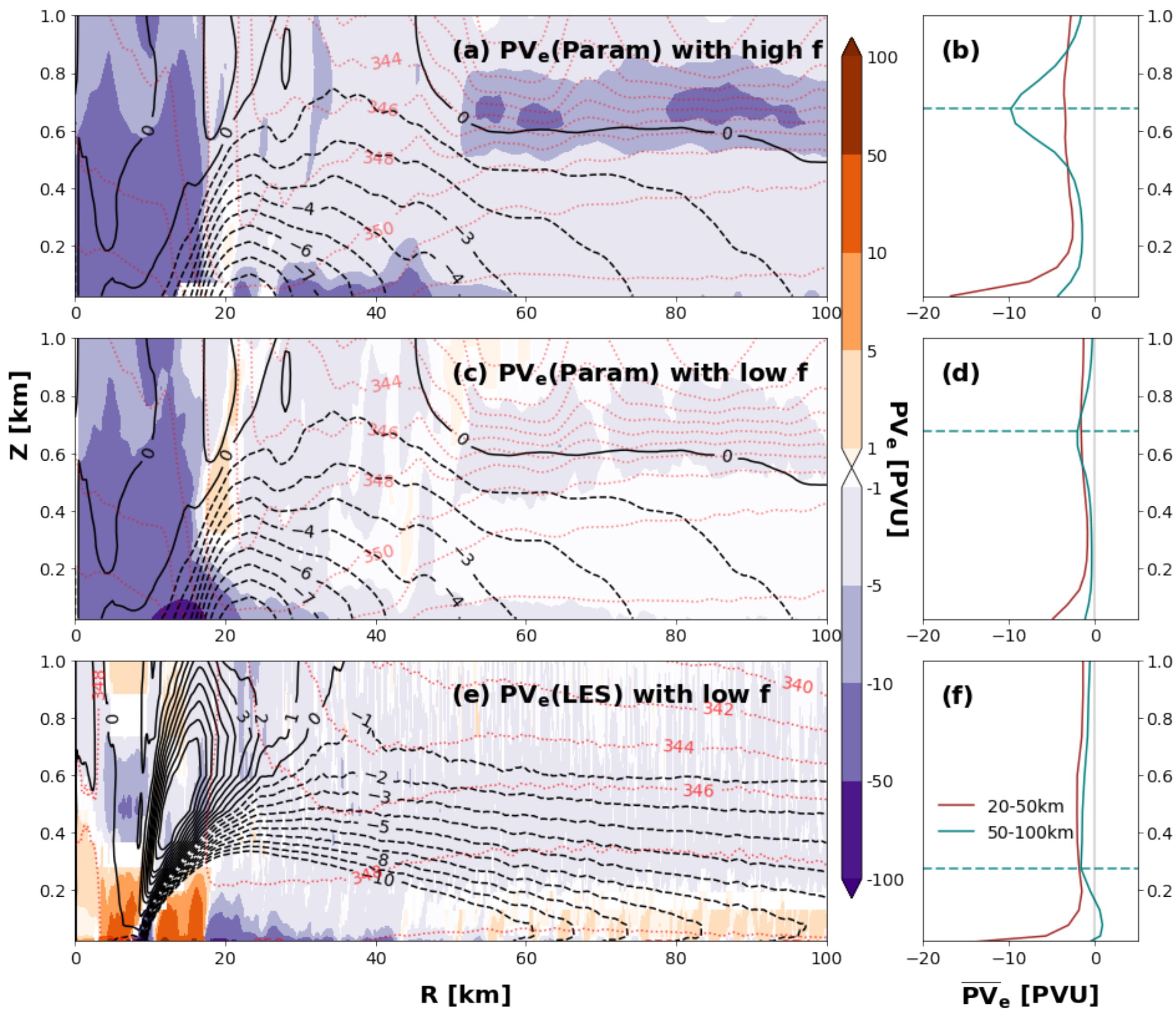

Figure 2. Radial-vertical distribution of PVe in TC-Param when computed with (a) original value of f (high) and (c) f used in TC-LES (low). The same has been plotted for (e) TC-LES to allow comparison of PVe magnitudes. The corresponding vertical profile of radially averaged in radial ranges of 20-50 km (red) and 50-100 km (green) are plotted in b,d,f. The green dashed line indicates the h_{PVML} in R=50-100 km.

Since the PV_e distribution outside of the eyewall is largely dominated by the planetary vorticity, we can divide the PVML magnitude by the original *f* and multiply with low f to get: $\frac{-10\ PVU}{0.0002}$x 0.000025 = -1.25 PVU, which is approximately the order of TC-LES PVML magnitude.

S3. In order to isolate regions with/without roll vortices, the TC-domains have been divided into several smaller sub-domains of size 10 km x 10 km x 1 km as shown in Figure 3.

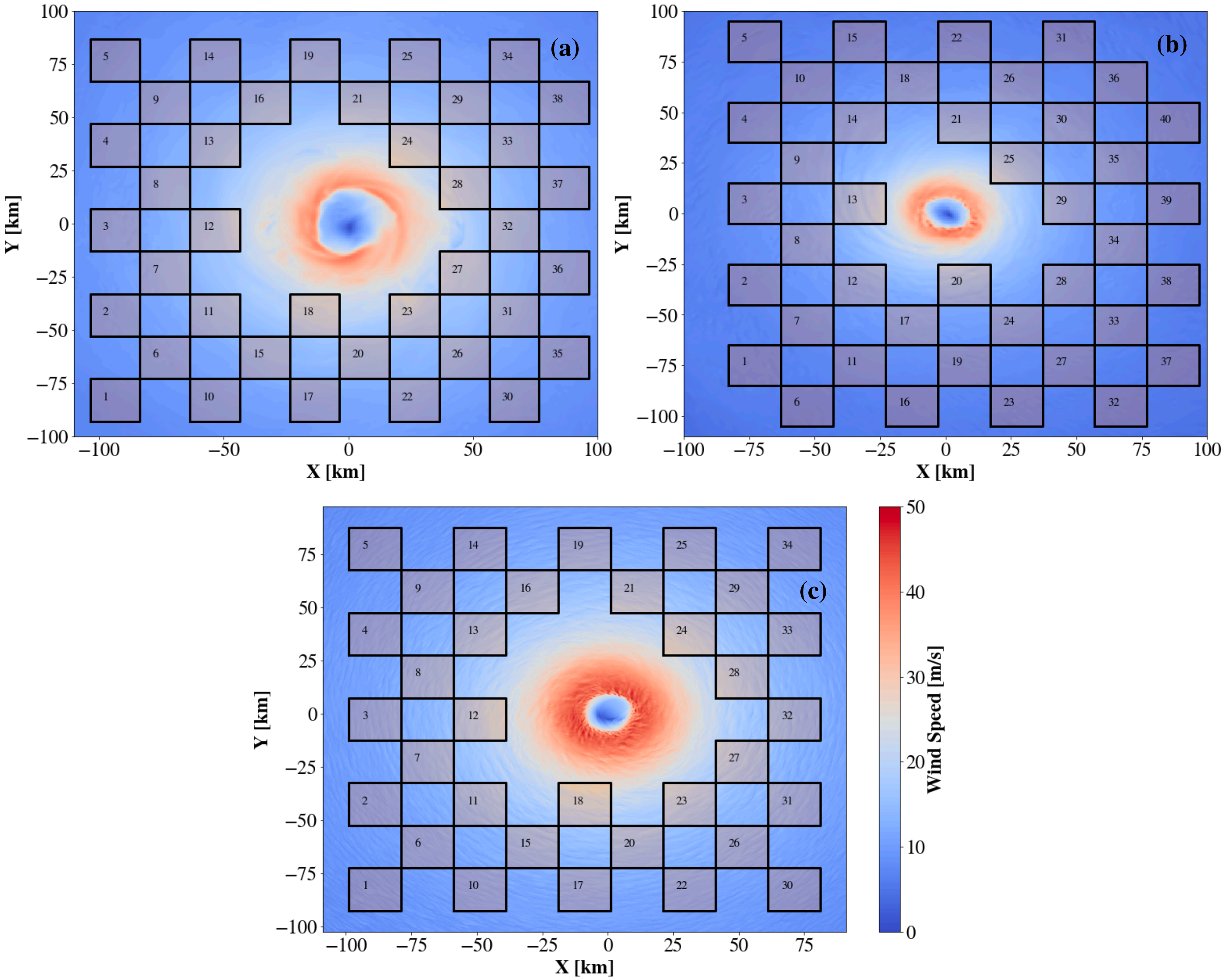

Figure 3. Horizontal wind speeds at the lowest model height for (a) TC-Param at t=199 h, (b) TC-NonParam at t=199 hr and (c) TC-LES at t=120.5 hr. The numbered boxes indicate the 10km x 10km sub-domains used for roll-identification.